

# Arecibo Pulsar Survey Using ALFA. III. Probing Radio Pulsar Intermittency and Transients

J. S. Deneva<sup>1,\*</sup>, J. M. Cordes<sup>1</sup>, M. A. McLaughlin<sup>2</sup>, D. J. Nice<sup>3</sup>, D. R. Lorimer<sup>2</sup>,  
 F. Crawford<sup>4</sup>, N. D. R. Bhat<sup>5</sup>, F. Camilo<sup>6</sup>, D. J. Champion<sup>7</sup>, P. C. C. Freire<sup>8,2</sup>, S. Edel<sup>2</sup>,  
 V. I. Kondratiev<sup>2</sup>, J. W. T. Hessels<sup>9</sup>, F. A. Jenet<sup>10</sup>, L. Kasian<sup>11</sup>, V. M. Kaspi<sup>12</sup>,  
 M. Kramer<sup>13</sup>, P. Lazarus<sup>12</sup>, S. M. Ransom<sup>14</sup>, I. H. Stairs<sup>11</sup>, B. W. Stappers<sup>13</sup>,  
 J. van Leeuwen<sup>15</sup>, A. Brazier<sup>1</sup>, A. Venkataraman<sup>8</sup>, and J. A. Zollweg<sup>16</sup>

November 15, 2019

<sup>1</sup>*Astronomy Dept., Cornell Univ., Ithaca, NY 14853*

<sup>2</sup>*Department of Physics, West Virginia Univ., Morgantown, WV 26506*

<sup>3</sup>*Physics Dept., Bryn Mawr College, Bryn Mawr, PA 19010*

<sup>4</sup>*Department of Physics and Astronomy, Franklin and Marshall College, P.O. Box 3003,  
 Lancaster, PA 17604-3003*

<sup>5</sup>*Centre for Astrophysics and Supercomputing, Swinburne Univ. of Technology, Hawthorn,  
 Victoria 3122, Australia*

<sup>6</sup>*Columbia Astrophysics Laboratory, Columbia Univ., New York, NY 10027*

<sup>7</sup>*ATNF-CSIRO, Epping, NSW 1710, Australia*

<sup>8</sup>*NAIC, Arecibo Observatory, PR 00612*

<sup>9</sup>*Astronomical Institute “Anton Pannekoek,” Univ. of Amsterdam, 1098 SJ Amsterdam,  
 The Netherlands*

<sup>10</sup>*Center for Gravitational Wave Astronomy, Univ. of Texas at Brownsville, TX 78520*

<sup>11</sup>*Dept. of Physics and Astronomy, Univ. of British Columbia, Vancouver, BC V6T 1Z1,  
 Canada*

<sup>12</sup>*Dept. of Physics, McGill Univ., Montreal, QC H3A 2T8, Canada*

<sup>13</sup>*Univ. of Manchester, Jodrell Bank Centre for Astrophysics, Alan Turing Building,  
 Manchester M13 9PL, UK*

<sup>14</sup>*NRAO, Charlottesville, VA 22903*

<sup>15</sup>*Stichting ASTRON, Postbus 2, 7990 AA Dwingeloo, The Netherlands*

<sup>16</sup>*Center for Advanced Computing, Cornell Univ., Ithaca, NY 14853*

*\*E-mail: deneva@astro.cornell.edu*

## ABSTRACT

We present radio transient search algorithms, results, and statistics from the ongoing Arecibo Pulsar ALFA (PALFA) Survey of the Galactic plane. We have discovered seven objects by detecting isolated dispersed pulses and one of the new discoveries has a duty cycle of 0.01%, the smallest known. The impact of selection effects on the detectability and classification of intermittent sources is discussed, and the relative efficiencies of periodicity vs. single pulse searches are compared for various pulsar classes. We find that scintillation, off-axis detection and few rotation periods within an observation may misrepresent normal periodic pulsars as intermittent sources. Finally, we derive constraints on transient pulse rate and flux density from the PALFA survey parameters and results.

## 1. Introduction

Radio pulsars show a wide variety of modulations of their pulse amplitudes, and these affect their detectability in surveys. Several types of intermittent neutron stars have been identified based on their pulse amplitude distributions and the fraction of time that periodic emission is observed. One such class consists of nulling pulsars, first discovered by Backer (1970). In these sources, the pulsed flux sharply decreases, typically in less than one spin period. Pulses are not detectable for several or many consecutive periods before the flux just as sharply increases back to its normal value. A subset of nulling pulsars exhibit more extreme behavior, with the pulsed emission remaining off 30 – 95% of the time (Deich et al. 1986, Lewandowski et al. 2004, Wang et al. 2006).

Pulsar eclipses are observationally similar to nulls in that the pulsar emission may be undetectable for stretches of time much longer than the pulsar period. Eclipses have been detected in the millisecond pulsars B1957+20 (Fruchter et al. 1988), J1744-24A (Lyne et al. 1990), J2051-0827 (Stappers et al. 1996) and J1740-5340 (D’Amico et al. 2001). The eclipses of the long-period pulsar B1718-19 are partial at frequencies  $\gtrsim 1.4$  GHz and full at lower frequencies (Lyne et al. 1993). Kaspi et al. (2004) observed eclipses with a frequency-dependent duration in the double pulsar binary J0737-3039.

Two other new transient pulsar classes have recently been reported: the intermittent pulsar B1931+24 (Kramer et al. 2006) and Rotating Radio Transients (McLaughlin et al.

2006). B1931+24 is on for  $\sim 5$  days, abruptly shuts off in less than 10 s and remains quiescent for 25-35 days at a time. The spin-down rate is 50% larger while the pulsed emission is on than when it is off, which can be explained by magnetospheric currents being much stronger during the “on” phase and affecting the spin-down torque.

Rotating Radio Transients (RRATs) are a phenomenological class of transient radio loud neutron stars emitting isolated bursts at intervals between a few minutes and a few hours first discovered in archival Parkes Multibeam survey data (McLaughlin et al. 2006). Eleven objects with periods ranging from 0.4 to 7 s and pulse widths of 2 – 30 ms were found using a single pulse search algorithm. The longer periods of RRATs compared with the general pulsar population suggest similarities with the X-ray populations of X-ray dim isolated neutron stars (XDINSs) and magnetars. RRAT J1819–1458 has been detected at X-ray energies (McLaughlin et al. 2007) with properties that are similar to those of XDINSs and high magnetic field radio pulsars.

A different type of pulse modulation is observed in the case of pulsars emitting giant pulses. Such pulses are tens to thousands of times brighter and an order of magnitude or more narrower than the average pulse (see Knight 2006 for an overview). Giant pulses from the Crab pulsar have substructure on timescales of 2 ns (Hankins et al. 2003), and B1937+21 emits giant pulses as narrow as 16 ns (Popov et al. 2004). Giant micro-pulses from the Vela pulsar have widths  $\sim 50\mu\text{s}$  (Johnston et al. 2001), and the slowly rotating pulsars B1112+50, B0031–07, and J1752+2359 occasionally emit bright pulses which are 1 – 10 ms wide, 5 – 30 times narrower than the average pulse (Knight 2006). The detection of giant pulses is a potentially powerful method for finding pulsars in regions with significant scattering and dispersion such as the Galactic Center, and for extragalactic pulsars too distant for their normal emission to be detectable by periodicity searches (McLaughlin & Cordes 2003).

A variety of energetic phenomena other than pulsar emission can give rise to fast transients potentially detectable in radio pulsar surveys. Within the Solar System, transient radio events may be generated by energetic particles impacting the Earth’s atmosphere, solar flares, and decameter radio flares originating in Jupiter’s atmosphere. Analogously to the latter, extrasolar planets with strong magnetic fields are expected to be detectable in the 10-1000 MHz range (Farrell et al. 1999, Lazio et al. 2004, Zarka et al. 2001). Magnetic activity on the surfaces of brown dwarfs and particle acceleration in the magnetic fields of flare stars are also known radio flare progenitors (Berger et al. 2001, Berger 2002, Garcia-Sanchez et al. 2003, Jackson et al. 1989). Gamma-ray bursts are predicted to have detectable radio emission at  $\sim 100$  MHz (Usov & Katz 2000, Sagiv & Waxman 2002), and radio flares have been observed from some X-ray binaries (Waltman et al. 1995, Fender et al. 1997). Among the most energetic and exotic events in the Universe, supernovae, merging neutron stars and coa-

lescings black holes may produce wide-band radio bursts detectable at extragalactic distances (Hansen & Lyutikov 2000).

In this paper we describe an ongoing survey for pulsars and transient radio sources with the Arecibo telescope. The survey addresses outstanding questions about the nature and emission mechanisms of intermittent radio sources. In § 2 we present the PALFA survey parameters, and in § 3 we describe the single pulse search and radio frequency interference excision algorithms which are part of the survey data processing pipeline. § 4 contrasts PALFA detection statistics on known pulsars and new discoveries, and § 5 examines selection effects influencing the detection and classification of transient sources. In § 6, we apply an intermittency measure method for comparing the efficiency of periodicity and single pulse pulsar searches. In § 7, we discuss the properties of individual intermittent objects discovered by PALFA. In § 8, we apply constraints derived from the survey sensitivity and results to the detectability of various energetic phenomena expected to emit radio bursts. Finally, in § 9, we present our main conclusions.

## 2. PALFA Survey Parameters

The PALFA survey started in 2004, shortly after the installation of the seven-beam ALFA receiver on the Arecibo telescope. The survey searches for pulsars and transients in the inner and outer Galactic plane regions accessible to Arecibo (see below). The survey has already made a number of discoveries, including the young pulsar J1928+1746 (Cordes et al. 2006), the relativistic binary J1906+0746 (Lorimer et al. 2006), the unusual, highly eccentric binary J1903+0327 (Champion et al. 2008), and the Vela-like pulsar J1856+0245 whose position coincides with a TeV gamma-ray HESS source (Hessels et al. 2008).

The ALFA receiver is well-suited for survey observations, allowing simultaneous data collection from seven fields, each  $\sim 3.5'$  (FWHM) across. Taking into account the hexagonal arrangement of the beams on the sky and the near sidelobes, the combined power-pattern is approximately  $24' \times 26'$  (Cordes et al. 2006). We observe a 100 MHz passband centered on 1440 MHz in each of the seven telescope beams. Wideband Arecibo Pulsar Processors (WAPPs) are used to synthesize 256-lag autocorrelations spanning these bands at intervals of  $64 \mu\text{s}$ .

Standard observation times are 268 s for inner Galaxy pointings ( $30^\circ \lesssim l \lesssim 78^\circ, |b| \leq 5^\circ$ ) and 134 s for outer Galaxy pointings ( $162^\circ \lesssim l \lesssim 214^\circ, |b| \leq 5^\circ$ ), with a sampling time of  $64 \mu\text{s}$ . Some early observations had a duration of 134 s and 67 s for inner and outer Galaxy pointings, respectively. Table 1 lists the area covered to date in both regions, as well as area

corresponding to processed and inspected data.

To compare the performance of the PALFA survey to the Parkes Multibeam survey (Manchester et al. 2001), we compare the maximum distance at which sources with various luminosities would be detectable,  $D_{\max}$ . Considering radio transients in particular, the effective observation time is equal to the pulse width  $W$ , and therefore the rms noise is

$$\sigma_n = \frac{S_{\text{sys}}}{\sqrt{N_{\text{pol}} \Delta f W}}, \quad (1)$$

where  $S_{\text{sys}}$  is the system-equivalent flux density,  $N_{\text{pol}} = 2$  is the number of polarization channels summed and  $\Delta f$  is the bandwidth.

A pulse’s observed width  $W$  may be broadened compared to its intrinsic width  $W_i$  by several effects. After dedispersing the raw data and obtaining a dedispersed time series, there is residual dispersive broadening due to the finite width of a frequency channel and the error of the trial dispersion measure (DM) used compared to the actual pulsar DM. Scatter broadening is not correctable and will have a contribution that depends on observing frequency and varies with direction on the sky. In general,

$$W = (W_i^2 + \Delta t_{\text{DM,ch}}^2 + \Delta t_{\text{DM,err}}^2 + \Delta t_{\text{sc}}^2)^{1/2}, \quad (2)$$

where  $\Delta t_{\text{DM,ch}} = 8.3 \mu\text{s DM} \Delta f_{\text{ch,MHz}} / f_{\text{GHz}}^3$  is the dispersive broadening across a frequency channel of width  $\Delta f_{\text{ch,MHz}}$  for an observing frequency  $f$ ,  $\Delta t_{\text{DM,err}}$  is the dispersive broadening due to the difference between the trial and actual DM of the source, and  $\Delta t_{\text{sc}} \propto f^{-4}$  is the scattering broadening. Broadening conserves pulse area, so that the intrinsic and observed peak flux densities are related through  $S_{\text{p,i}} W_i = S_{\text{p}} W$ . If  $S_{\text{p,min}} = m \sigma_n$  is the detection threshold, the minimum detectable peak flux density is

$$S_{\text{p,i,min}} = \left( \frac{W}{W_i} \right) \frac{m S_{\text{sys}}}{\sqrt{N_{\text{pol}} \Delta f W}}. \quad (3)$$

Table 1. PALFA survey statistics: area in square degrees.

	Inner Galaxy	Anticenter
Observed	156	119
Processed	99	87

A source of intrinsic peak luminosity  $L_{p,i}$  can be detected out to a maximum distance of

$$D_{\max} = \left( \frac{L_{p,i}}{S_{p,\min}} \right)^{1/2} = L_{p,i}^{1/2} \left( \frac{W_i}{W} \right)^{1/2} \frac{(N_{\text{pol}} \Delta f W)^{1/4}}{(m S_{\text{sys}})^{1/2}}. \quad (4)$$

For a steadily emitting pulsar with period-averaged luminosity  $L$  and duty cycle  $f_{\text{dc}}$ , we have  $L_p \approx L/f_{\text{dc}}$ .

The amount of pulse broadening depends on system parameters as well as dispersion and scattering, which vary with direction on the sky so that  $W = W(W_i, l, b, f, \Delta f, N_{\text{ch}}, S_{\text{sys}}, \Delta t)$ . We use the NE2001 model of Galactic ionized electron density (Cordes & Lazio 2002) to calculate representative results for  $D_{\max}$  in the direction  $l = 35^\circ, b = 0^\circ$ , a region of overlap between PALFA and the Parkes Multibeam survey. Fig. 1 shows  $D_{\max}$  vs.  $L_p$  detection curves for both surveys. For lower luminosities, sources are not visible to large enough distances for scattering to affect detectability and the inverse square law dominates the detection curve so that  $D_{\max} \propto L_p^{1/2}$ . For larger distances and smaller intrinsic pulse widths, scattering makes pulses increasingly hard to detect and  $D_{\max}$  increases more slowly with  $L_p$ .

### 3. Single Pulse Search Methods

We dedisperse raw data with 1272 trial DMs in the range  $0 - 1000 \text{ pc cm}^{-3}$ . In order to find individual pulses from intermittent sources we operate on dedispersed time series with two time domain algorithms: matched filtering, which has been the standard in single pulse searching so far, and a friends-of-friends algorithm. After single pulse candidates have been identified we use a stacking method in the time-frequency plane to verify that the pulses are dispersed and the sweep observed across frequencies follows the dispersion relation, as expected for non-terrestrial sources.

#### 3.1. Matched Filtering

Matched filtering detection of broadened pulses relies on the convolution of a pulse template with the dedispersed time series. Ideally, a pulse template would consist of one or several superimposed Gaussian templates, reflecting the diversity of pulsar pulse profiles, some of which exhibit multiple peaks. In addition, multipath propagation due to scattering adds an exponential tail to the pulse profile. We approximate true matched filtering by smoothing the time series by adding up to  $2^n$  neighboring samples, where  $n = 0 - 7$ , and selecting events above a threshold after each smoothing iteration. The smoothing is done in pairs of samples at each  $n$ -stage, so that the resulting template is a boxcar of length  $2^n$

samples. The sampling time used in PALFA observations is  $64 \mu\text{s}$  and therefore our matched filtering search is most sensitive to pulse widths of  $64 \mu\text{s}$  to  $8.2 \text{ ms}$ . This search strategy is not optimal for single pulses from heavily scattered pulsars because the templates are symmetric, while the scattered pulse shape with an exponential tail is not, and significantly scattered pulses can be wider than  $\sim 10 \text{ ms}$ .

### 3.2. Friends of Friends

Two issues make a complement to matched filtering necessary. The pulse templates described above have discrete widths of  $2^n$  samples by algorithm design and there is decreased sensitivity to pulses with widths that are significantly different. In addition, the matched filter search output may be dominated by bright, wide pulses from radio frequency interference (RFI). In that case, a single RFI burst is detected as an overwhelming number of individual events instead of a single event. The friends-of-friends search algorithm (Huchra & Geller 1982) complements matched filtering by not restricting the width of expected pulse detections. The dedispersed time series is processed sequentially and if an event above a threshold is found, it is designated as the first of a cluster. A cluster of events is augmented while successive samples are found to be above a threshold. The brightest sample of a cluster is recorded as the event amplitude, and the total number of samples in the cluster as its width. This approach is less sensitive to weak, narrow pulses but results in significantly fewer spurious events due to RFI.

A limiting factor for the largest pulse width detectable by both the matched filtering and friends-of-friends search algorithms is the fact that data are analysed in blocks much shorter than the complete time series length. The mean and standard deviation of a block are used for thresholding events found within the block. This approach minimizes the effect of baseline variations with time scales much longer than typical pulsar pulse widths of a few to a few tens of ms. The disadvantage is that only pulses with  $W \ll T_{\text{block}}$  can be detected. In processing PALFA data, we use blocks of length  $T_{\text{block}} = 4096 \times 64 \mu\text{s} = 0.26 \text{ s}$ . According to the NE2001 model of ionized gas in the Galaxy (Cordes & Lazio 2002), a scattering broadening time of that magnitude in the inner Galaxy part of the PALFA survey corresponds to  $\text{DM} > 1000 \text{ pc cm}^{-3}$  and a maximum search distance well outside of the Milky Way for most directions we survey. However, lines of sight intersecting HII regions can result in large dispersion measures and scattering times and are therefore selected against.

### 3.3. Example Results

Fig. 2 shows standard single pulse search output for the discovery observation of J0627+16 (§ 8.1). The main panel shows signal-to-noise ratio (S/N) vs. DM and time for events with  $S/N > 5$ . The panels on top illustrate event statistics for the observation: from left to right, number of events vs. S/N and DM, and DM vs. S/N. The pulsar detection is manifested as a peak in the histogram of number of events vs. DM. There is a corresponding peak in the DM vs. S/N plot, since the several detected pulses are significantly brighter than background noise in the dedispersed time series.

Fig. 3 shows events in DM-time space for another PALFA single pulse discovery, J1928+15 (§ 8.5). In this case, three closely spaced bursts were found at  $t \sim 100$  s,  $DM \sim 250$  pc cm<sup>-3</sup>. The pulsar is detected at a range of DMs, with the signal to noise ratio increasing as trial DM values approach the actual pulsar DM and decreasing as trial DMs further on recede from the pulsar DM. In contrast, events due to radar RFI at  $t \sim 46, 82, 90, 118$  s span the entire range of trial DMs and their signal to noise ratios do not show a significant variation with DM.

If an excess of candidate pulses is identified in the dedispersed time series for a particular trial DM, we use the expected dispersion sweep across the frequency band in order to test if the pulses are from non-terrestrial origin. For a pulse with  $S/N \gtrsim 10$  in the time series, we extract a chunk of raw data centered on its time of arrival and look for a sweep across frequency that follows the dispersion relation (Fig. 4 a, b).

### 3.4. Time-Frequency Plane Stacking

In the case of multiple weaker pulses detected in the same beam, we extract a raw data chunk centered on the arrival time of each pulse, stack the chunks and look for a dispersion sweep in the resulting cumulative dynamic spectrum (Fig. 4 c, d).

Since the time-frequency plane contains mostly Gaussian noise, stacking can result in spurious events in the dedispersed time series due to unassociated bright points in the time-frequency plane being summed during dedispersion. We performed a simulation of this effect by generating a time-frequency plane of Gaussian noise, dedispersing it, and selecting events above a threshold from the resulting time series. We extracted chunks from the fake time-frequency plane centered on each event and stacked them, thus reproducing the procedure for verifying the dispersive sweep of stacked weak pulses. We found that if a large enough number of noise-only chunks are added, this produces a spurious pulse in the cumulative dynamic spectrum which follows the dispersion relation because it results from summing



chunks centered on unrelated bright points in the time-frequency plane that happened to line up during dedispersion. In general, a spurious pulse is seen if:

$$N_r > (m_c/m_d)^2 N_{\text{ch}}, \quad (5)$$

where  $N_r$  is the number of chunks (“realizations”) added,  $N_{\text{ch}}$  is the number of frequency channels, and  $m_d$  is the event S/N in the dedispersed time series above which a raw data chunk centered on the event will be extracted and used in the stacking.  $m_c$  is the S/N of a point at a particular time sample and frequency channel in the cumulative dynamic spectrum defined with respect to the channel noise, such that if there is a contiguous swath of points, each with  $S/N = m_c$ , the swath would be just barely visible to the eye.

For the PALFA survey and our processing pipeline,  $N_{\text{ch}} = 256$ ,  $m_c \sim 2$ , and  $m_d = 5$ . Therefore if  $N_r \gtrsim 40$  data chunks aligned around events above threshold in the dedispersed time series are added, there will be a spurious pulse in the cumulative dynamic spectrum even if the chunks contain only noise. Since the added noise decorrelates over 1 – 2 samples, the pulse will have a width on the order of 64 – 128  $\mu\text{s}$ . In the case of J1909+06 (Fig. 4d) only 2 chunks were added and the dispersed swath in the time-frequency plane is 1 ms wide. Typically we sum chunks centered on the brightest 2 – 5 pulses for a single pulse candidate, which is safely below the  $N_r$  limit.

### 3.5. RFI Excision

The RFI environment at the Arecibo telescope and the 7-beam configuration of the ALFA receiver present both challenges and opportunities for RFI mitigation to facilitate searching for single pulses. PALFA survey data is dedispersed with trial dispersion measures of 0 – 1000  $\text{pc cm}^{-3}$ . RFI pulse intensity typically peaks at  $\text{DM} = 0 \text{ pc cm}^{-3}$  and incidental low-intensity pulses whose S/N peaks at  $\text{DM} = 0 \text{ pc cm}^{-3}$  tend to be smeared below the detection threshold for dedispersed time series with trial  $\text{DM} > 50 - 100 \text{ pc cm}^{-3}$ . A more complex signature is observed for Federal Aviation Administration (San Juan airport) radar pulses, which are unfortunately common in Arecibo observations. The radar rotation period is  $P_r = 12 \text{ s}$ , and each pulse has an envelope that is  $\sim 1 \text{ s}$  wide and consists of sub-pulses with variable period on the order of 2 – 3 ms. Depending on telescope orientation, radar pulses may be detected in all, some, or none of the ALFA beams due to reflections off the telescope structure. Radar pulses are up to two orders of magnitude brighter than pulsar pulses and, without mitigation, can completely dominate single pulse search results. In addition, the modulation of the radar signal is manifested as detections with  $\text{DM} \neq 0 \text{ pc cm}^{-3}$  so that unlike other non-radar RFI, their S/N vs. DM signature cannot be used for excision.

We exploit the known radar characteristics as well as the pattern of pulse detection in the 7 ALFA beams to excise both radar and non-radar RFI. The first part of our excision algorithm targets radar pulses. After a list of single pulse events is generated for all trial DMs, we bin the events for trial  $DM = 0 - 3 \text{ pc cm}^{-3}$  in time (by 0.1 s) and record the number of events in each time bin. Then we treat the histogram as a time series and perform a discrete Fourier transform. A peak near the radar rotation frequency indicates a significant number of radar pulses in the data. From the Fourier components we extract the phase and find the arrival time of the earliest radar pulse,  $t_0$ . Since the envelope width is  $\sim 1$  s, events within 0.5 s of that location are excised, and the procedure is repeated for events near  $t = t_0 + NP_r$ , where  $N$  is an integer. The more radar pulses are present, the better the performance of this technique because the radar peak in the DFT is more prominent and the pulses' arrival times are determined more precisely. However, if only a couple of strong radar pulses are present within the typical 268 s PALFA integration time, they may be bright enough to dominate event statistics, yet the DFT method does not excise non-periodic incidental RFI. Consequently, after applying the DFT-based method we use an additional RFI filter that handles aperiodic cases.

The second filter uses the number and proximity of beams in which an event is detected in order to determine if it is due to RFI. Again events for trial  $DM = 0 - 3 \text{ pc cm}^{-3}$  from each beam are binned in time. After detecting peaks indicating an excess of events for the respective time bins, the algorithm cross-checks between results for all 7 beams and each event falling within a histogram peak receives a penalty grade based on how many beams' histograms exhibit a peak, and how close to each other they are on the sky. Most pulsars detected blindly via a single pulse search appear in one beam or two adjacent beams, and very bright pulsars may be detected in three or four adjacent beams. We set the excision penalty threshold just below the value corresponding to the latter configurations and excise events accordingly. This method complements the DFT cleaning scheme and effectively excises sparse radar blasts as well as non-periodic RFI detected in multiple beams. The application of the two excision algorithms makes a marked difference in the final single pulse search output for pointings contaminated with RFI (Fig. 5).

#### 4. PALFA Pulsar Detection Statistics

The PALFA survey has made a total of 354 blind detections of 172 pulsars up to late 2008. Following a low-resolution processing of the data for long-period pulsars shortly after the data are acquired (Cordes et al. 2006), data are shipped to external sites for processing

through the Cornell pulsar search code and PRESTO <sup>1</sup>. Table 2 shows a breakdown of Cornell detections by the periodicity (FFT) and single pulse (SP) search algorithms for known pulsars and new discoveries, and Table 3 lists parameters for PALFA single pulse discoveries discussed in more detail in § 7.

More than half of the detected known pulsars and only a quarter of the newly discovered objects were seen by both the periodicity and single pulse search algorithms. There is also a significant difference in the fraction of pulsars detected only via a single pulse search. In total, 74% of the new pulsars were detected either only by FFT search or only by single pulse search, as opposed to 42% of the known pulsars. This illustrates that PALFA is probing deeper than previous surveys and finding pulsars which are farther away or less bright than the known objects in the same region of the Galactic plane. Single pulse searches have not been routinely carried out on survey data in the past, with the exception of Phinney & Taylor (1979) and Nice (1999), who discovered J1918+08 via a single pulse search. Therefore, the proportion of single-pulse-only detections is higher for the PALFA discoveries than the known pulsars. The five known pulsars detected only by single pulse search are known steady emitters which were seen away from the beam center and therefore with reduced sensitivity.

## 5. Selection Effects and Intermittency

The sample of PALFA single pulse discoveries (§ 7) includes one object which has not been detected again despite reobservations (J1928+15), two sources with consistent periodic emission revealed after reobservation (J0628+09 and J1909+06), and four long-period objects, one of which may have giant pulse emission.

Among the 11 Parkes RRATs, 10 were successfully reobserved, and one (J1839–01)

---

<sup>1</sup><http://www.cv.nrao.edu/~sransom/presto>

Table 2. Pulsar detection statistics by algorithm.

Pulsars	FFT only	SP only	FFT and SP	Total
Known	48 (38%)	5 (4%)	73 (58%)	126
New	28 (61%)	6 (13%)	12 (26%)	46

Table 3. Parameters of PALFA single pulse discoveries: period, FWHM pulse width, dispersion measure, estimated distance, peak flux density of the brightest detected pulse, total observation time, total pulses detected, and average pulse rate.

Pulsar	$P$ (s)	$W$ (ms)	DM (pc cm <sup>-3</sup> )	$D$ <sup>a</sup> (kpc)	$S_p$ <sup>b</sup> (mJy)	$T_{\text{tot}}$ (s)	$N_{\text{tot}}$	Rate (h <sup>-1</sup> )	Comment
J0627+16	2.180	0.3	113	3.2	150	7454	48	23	§ 7.1
J0628+09	1.241	10	88	2.5	85	1072	42	141	§ 7.2
J1854+03	4.559	80 <sup>c</sup>	216	5.5	9	388	9	84	§ 7.3
J1909+06	0.741	1.5	35	2.2	82	536	10	67	§ 7.4
J1919+17	2.081	100	148	5.3	12	393	35	320	§ 7.5
J1928+15	0.403	5	242	7.4	180	2880	3	4	§ 7.6
J1946+24	4.729	4	96	4.3	101	268	4	54	§ 7.7

<sup>a</sup> Estimate from the NE2001 model of Galactic electron density (Cordes & Lazio 2002).

<sup>b</sup> Peak flux density at 1.4 GHz defined as  $S = (S/N)S_{\text{sys}}/\sqrt{N_{\text{pol}}\Delta fW}$ , where  $S/N$  is the signal to noise ratio of the brightest detected pulse.

<sup>c</sup> Estimate from fitting S/N vs  $\delta\text{DM}$  (§ 7.1).

has not been redetected despite multiple attempts. Some RRATs show consistent periodic emission in addition to strong single pulses: for example, consistent periodic emission was detected from Parkes sources J0848–43 and J1754–30 when they were observed with the Green Bank Telescope at low frequency (McLaughlin 2008, private communication). Six of the sources have periods greater than 2 s and four of these long-period sources have the smallest duty cycles in the Australia Telescope National Facility (ATNF) pulsar catalog<sup>2</sup> (Manchester et al. 2005).

In this section we discuss selection effects which may account for some of the observational characteristics of intermittent sources. Characteristics of this population which remain unexplained by observational biases may indicate underlying intrinsic differences between these objects and conventional radio pulsars. They may belong to a genuinely intermittent and physically different class of neutron stars.

### 5.1. Multiplicative Effects

We can define a general model for observed signal intensity in terms of the time and frequency-dependent flux density  $S_i(t, \nu)$  as

$$I(t, \nu) = G_t(t, \nu) G_{\text{ISS}}(t, \nu) S_i(t, \nu) + n(t, \nu) + \text{RFI}(t, \nu), \quad (6)$$

where  $G_t$  is the telescope gain,  $G_{\text{ISS}}$  is the variation factor due to interstellar scintillation,  $n(t, \nu)$  is radiometer noise, and  $\text{RFI}(t, \nu)$  is the contribution from terrestrial radio frequency interference.

Variations in telescope gain across the beams of the multi-beam receiver or within the power pattern of a single beam impact the detectability of a pulsar as either a single pulse or periodic source. As shown by the reobservations of J0627+16, J1909+06, J0848–43 and J1754–30, classifying a source as intermittent may be due to insufficient sensitivity to detect its periodic emission during the discovery observation. The effectiveness of single pulse vs. FFT-based periodic search depends on the pulse amplitude distribution and the observed pulse amplitude distribution in turn depends on the pulsar location with respect to the telescope beam power pattern. Fig. 6 shows pulse intensity distributions for B1933+16, a strong pulsar detected in two beams of the same PALFA pointing. One beam of the ALFA receiver is pointing directly at the pulsar and the low-intensity tail of the distribution is clearly visible since all pulses are above the detection threshold. The pulsar is also detected

---

<sup>2</sup><http://www.atnf.csiro.au/research/pulsar/psrcat>

in the first sidelobe of an adjacent beam, in which case only the brightest pulses are above the detection threshold and only the high-intensity tail of the distribution is visible. Thus an off-axis detection of a steadily emitting pulsar may misrepresent it as an intermittent source.

A different set of effects which affect detectability in single pulse vs. periodic search is due to intervening ionized gas. Turbulence in the ionized interstellar gas and the motion of the pulsar with respect to the gas introduce phase modulations in the pulsar emission which cause the observed intensity to change over time and frequency. The detectability of nearby pulsars with low DMs is affected by interstellar scintillation. The scintillation bandwidth  $\Delta f_{\text{ISS}}$  and scattering timescale  $\tau_s$  are related through  $2\pi\Delta f_{\text{ISS}}\tau_s \approx 1$ . An empirical fit from Bhat et al. (2004) for  $f$  in GHz and  $\tau_s$  in ms gives an estimate for  $\tau_s$  based on DM:

$$\log \tau_s = -6.46 + 0.154 \log \text{DM} + 1.07 (\log \text{DM})^2 - 3.86 \log f, \quad (7)$$

but there is significant scatter about this relationship. The transverse speed of the pulsar can be related to  $\Delta f_{\text{ISS}}$ , the scintillation time scale  $\Delta t_{\text{ISS}}$  and the pulsar distance  $d$  through

$$V_{\text{ISS}} = A \left( \frac{d}{\text{kpc}} \right)^{1/2} \left( \frac{\Delta f_{\text{ISS}}}{\text{MHz}} \right)^{1/2} \left( \frac{f}{\text{GHz}} \right)^{-1} \left( \frac{\Delta t_{\text{ISS}}}{\text{s}} \right)^{-1}, \quad (8)$$

where  $A = 2.53 \times 10^4 \text{ km s}^{-1}$  (Cordes & Rickett 1998, Gupta 1995). We make use of these relations in § 7.4 to calculate  $\Delta t_{\text{ISS}}$  for the PALFA single pulse discovery J1909+06.

## 5.2. Observation Time vs Pulsar Period

The detectability of a pulsar as a periodic source depends on the number of periods within an observation,  $N_p = T_{\text{obs}}/P$ , along with the pulse amplitude distribution. We explore this dependency by simulating the results of an FFT-based search of periodic trains of Gaussian-shaped pulses with a varying fraction of pulses on,  $f_{\text{on}}$ . For an integration time  $T_{\text{obs}}$ , pulse period  $P$ , amplitudes  $A_k$  (where  $k$  is the pulse number) and width  $W$ , after adding  $N_h$  harmonics, the normalized harmonic sum is

$$H(N_h) = \frac{W}{2\sqrt{N_h}} \sum_{n=1}^{N_h} \exp \left[ -\frac{\pi^2 W^2 n^2}{2P^2} \right] \sum_{k=1}^{T_{\text{obs}}/P} A_k. \quad (9)$$

$H(N_h)$  is a figure of merit for detecting periodic pulsars and is typically the quantity on which a threshold is applied in periodicity searches. Fig. 7 shows contours of  $H(N_h)$  vs.  $P$  and  $f_{\text{on}}$  for  $T_{\text{obs}} = 268 \text{ s}$ ,  $N_h = 1 - 16$  (the value giving the highest  $H(N_h)$  is chosen),

$W = 1$  ms,  $P = 0.004 - 2$  s and  $A_k = 1$  or 0 depending on whether the  $k$ -th pulse is on or off. The small- $N_p$  bias becomes much more pronounced if  $< 50\%$  of pulses are on. Even if all pulses are on, pulsars with  $P \gtrsim 1.5$  s get increasingly harder to detect as periodic sources with the chosen integration time. Of five long-period pulsars discovered by PALFA, two were found in the periodicity search ( $P = 2.3$  and  $2.9$  s) and three via a single pulse search ( $P = 2.1, 4.5$  and  $4.7$  s). The harmonic sum simulation results suggest that the latter are likely normal periodic emitters not detected in the periodicity search because of the small number of periods within the standard PALFA integration time.

## 6. Intermittency Measure

Both the periodicity and single pulse searches perform with varying efficiency depending on an object’s degree of intermittency. In this section we present an intermittency measure method to quantify the relative performance of the two search algorithms, apply it to results from the Parkes Multibeam and PALFA surveys, and discuss general implications for surveys.

### 6.1. Definition

We can compare the detectability of objects by periodicity and single pulse search and attempt to narrow down different classes of intermittent emitters by calculating the intermittency ratio

$$r = (S/N)_{\text{SP}} / (S/N)_{\text{FFT}} \quad (10)$$

for each object in our sample of PALFA and Parkes detections. McLaughlin & Cordes (2003) derive

$$r = \left( \frac{2\eta}{\zeta N_p^{1/2}} \right) \frac{S_{\text{max}}}{S'_{\text{av}}}, \quad (11)$$

where  $\zeta \approx 1.06$  and  $\eta \sim 1$  for a Gaussian pulse shape,  $S_{\text{max}}$  is the maximum expected pulse intensity within  $N_p = T_{\text{obs}}/P$  periods and  $S'_{\text{av}}$  is a modified average pulse peak intensity.

The intermittency ratio is a system-independent measure of the efficiency of the two types of search for objects with different degrees of intermittency. In Fig. 8,  $r$  is shown vs.  $N_p$  for 283 PALFA pulsar detections, 255 Parkes Multibeam detections, and 10 of the 11 Parkes intermittent sources whose periods are known, along with expected values for  $r$  for an exponential pulse intensity distribution and power-law distributions with various indices. Lower limits on  $r$  are given for sources which were not detected via periodicity search.

## 6.2. Implications for Surveys

In Fig. 8 long-period pulsars are predominantly found in the upper left (small  $N_p$ , large  $r$ ) and millisecond pulsars in the lower right (large  $N_p$ , small  $r$ ). B0525+21, with  $r \sim 7$ , has  $P = 3.7$  s and  $DM = 51$  pc cm<sup>-3</sup>, which make it susceptible to both the small- $N_p$  and scintillation biases and therefore it is detected more readily as a single pulse source. At the other extreme is B1937+21, a millisecond pulsar which emits giant pulses but is nevertheless detected with a much higher S/N in the periodicity search than in the single pulse search ( $r < 0.07$ ) because its period is small compared to the PALFA observation time and the pulse amplitude is very steady. This indicates that the effect of  $N_p$  on detectability can overshadow individual properties, and in survey mode millisecond pulsars will show up overwhelmingly as periodic sources. In that case, processing the data with a single pulse search algorithm can reveal the presence of giant pulses in an otherwise steady emitter.

In-between B0525+21 and B1937+21, from upper left to lower right is a relatively smooth distribution of pulsars whose intermittency ratios are predominantly determined by the influence of  $N_p$  on the detectability of all types of periodic emitters. We look for unusual objects among the outliers from that trend. There are a number of pulsars detected both in periodicity and single pulse search in the region where  $r = 1 - 5$ , including the proposed nearby RRAT B0656+14 (Weltevrede et al. 2006). Interspersed among them in the region are most of the PALFA and Parkes intermittent sources. In particular, J1909+06 which was not detected in a periodicity search but is visible as a scintillating periodic source when folded with its known period has  $r = 1.3$  and the long-period PALFA intermittent sources J1854+03 and J1946+24 have  $r = 1.0$  and 1.8, respectively. Of the Parkes intermittent sources, seven have  $r < 3$ , J1754–30 ( $r = 0.2$ ) and J0848–43 ( $r = 0.7$ ) were detected as normal periodic emitters in follow-up observations, and J1839–01 does not have a period measurement to place it in  $r - N_p$  space. In the  $r > 5$  region we find only five objects: B0525+21, the Crab pulsar, Parkes intermittent sources J1317–5759 and J1819–1458, and PALFA intermittent source J1928+15. The Crab pulsar has a high intermittency ratio due to its giant pulses but is otherwise a steady emitter. Of the remaining three intermittent sources none are young pulsars and their pulse widths of a few milliseconds rule out giant pulse emission. The pulse amplitude distributions of J1317–5759 and J1819–1458 are described by power laws with indices  $\sim 1$  (McLaughlin et al. 2006), smaller than measured giant pulse indices of 2–3.

## 7. Single Pulse Discoveries

Table 3 lists parameters of the seven pulsars discovered by PALFA via a single pulse search. In this section we discuss each object’s properties in detail and describe the steps



taken in addition to the PALFA processing pipeline in order to verify the signals’ celestial origin and calculate the pulsar period from times of arrival of single pulses.

### 7.1. J0627+16

PSR J0627+16 was discovered when nine single pulses were detected at a trial  $DM = 125 \text{ pc cm}^{-3}$  (Fig. 2). The period estimated from the pulse arrival times in the discovery observation is  $P = 2.180 \text{ s}$ . What is unusual about this object is its very narrow peak in  $S/N$  vs.  $DM$  space. The expected relative signal to noise ratio for an error in trial  $DM$ ,  $\delta DM$ , is  $(S/N)_{\delta DM}/(S/N) \propto \text{Erf}(\zeta)/\zeta$ , where  $\zeta = 6.91 \times 10^{-3} \delta DM \Delta f_{\text{MHz}}/(W_{\text{ms}} f_{\text{GHz}}^3)$  (Cordes & McLaughlin 2003). A fit for J0627+16 yields  $W \approx 2 \text{ ms}$ . Fig. 4c shows the cumulative dynamic spectrum after stacking raw data chunks aligned around the five brightest pulses. A fit to the dispersion sweep in the time-frequency plane gives a best  $DM$  of  $113 \text{ pc cm}^{-3}$  and when the raw data chunk around the brightest pulse is dedispersed with this  $DM$ , the FWHM pulse width is only  $0.3 \text{ ms}$ . The discrepancy between the measured  $0.3 \text{ ms}$  width of the brightest pulse and the  $2 \text{ ms}$  pulse width estimated from the  $S/N$  vs.  $DM$  histogram is due to the fact that the latter is an average over the nine detected pulses. The individual pulse  $S/N$  vs. trial  $DM$  signature may vary slightly between pulses because of patchiness across frequency (Fig. 4c) and noise.

Two follow-up observations at  $0.33$  and  $1.4 \text{ GHz}$  yielded  $17$  pulses in  $50$  minutes and  $22$  pulses in  $72$  minutes, respectively. Consistent periodic emission with  $P = 2.180 \text{ s}$  was detected in search mode at  $0.33 \text{ GHz}$ , confirming the period estimate from the discovery observation. Repeating the time-of-arrival analysis on the  $1.4 \text{ GHz}$  observation gave a period estimate of  $1.095 \text{ s}$  and a weak periodic signal was detected when the raw data was folded with this period. The  $\sim P/2$  estimate from the  $1.4 \text{ GHz}$  follow-up observation suggests that there may be a weak frequency-dependent interpulse.

A period longer than the average for the normal pulsar population and a very short duty cycle are characteristic of RRATs. J0627+16 has the smallest known duty cycle,  $f_{\text{dc}} = 0.01\%$ . The detection of bright single pulses and a weak periodic signal from J0627+16 when data is manually folded with an accurate period estimate, along with the absence of a periodic detection in search mode weighs in favor of the proposition of Weltevrede et al. (2006) that some RRATs may have consistent periodic emission.

## 7.2. J0628+09

PSR J0628+09 was discovered by detecting three pulses at  $DM = 88 \text{ pc cm}^{-3}$ . The period estimated from the pulse times of arrival was 2.48 s. In follow-up observations the pulsar was also detected in periodicity searches as it emits on average several bursts per minute. The periodicity detections and the larger number of single pulses in subsequent observations allowed the actual pulsar period of 1.241 s to be determined (Cordes et al. 2006).

## 7.3. J1854+03

PSR J1854+03 was discovered in 2008 via a single pulse search performed on full-resolution survey data. Four pulses were detected at  $DM = 216 \text{ pc cm}^{-3}$  during the 268 s observation. The period  $P = 4.559 \text{ s}$  was estimated by taking the smallest difference between times of arrival (TOAs) of two pulses and verifying that intervals between all four TOAs are integer multiples of it. A confirmation observation with the more sensitive central ALFA beam yielded within 120 s five pulses whose arrival times match the estimated period.

## 7.4. J1909+06

PSR J1909+06 was observed in 2006 but not identified as a candidate until 2007 when the full-resolution data were searched for single pulses. Two pulses with a width of  $\sim 1 \text{ ms}$  and signal to noise ratio of 6 and 9 were detected at  $DM = 35 \text{ pc cm}^{-3}$ . In order to confirm their celestial origin, we extracted chunks from the time-frequency plane aligned around the pulses, and normalized and averaged the chunks. The resulting “cumulative” dynamic spectrum clearly shows a dispersion sweep (Fig. 4d). J1909+06 was discovered in data from the off-axis beam 2 of the multi-beam ALFA receiver. Since the on-axis gain of the center beam is 10.4 K/Jy compared to 8.2 K/Jy for the other six beams (Cordes et al. 2006), we aimed the center beam at the discovery coordinates for a confirmation observation. For the same integration time of 268 s, 8 pulses with  $S/N > 5$  were detected in the confirmation observation. We used the pulse arrival times to determine a period and arrived at a best estimate of  $P = 0.741 \text{ s}$ . Although the pulsar’s periodicity signature was not detected in search mode, after folding the confirmation observation with the period estimated from single pulse arrival times, it was also detected as a periodic emitter.

Following Eqn. 7, we estimate  $\tau_s$  the measured pulsar DM. The relation  $2\pi\Delta f_{\text{ISS}}\tau_s \approx 1$  gives  $\Delta f_{\text{ISS}} = 3 \text{ MHz}$  for J1909+06. From the NE2001 model of electron density in the

Galaxy (Cordes & Lazio 2002) we obtain  $d = 2.2$  kpc. Assuming a fiducial velocity  $V_{\text{ISS}} = 100 \text{ km s}^{-1}$  and using Eqn. 8, we get  $\Delta t_{\text{ISS}} = 450$  s. This is  $\sim 4$  times larger than the observed periodic emission variation time scale but roughly the same order of magnitude, which suggests that scintillation may contribute to the difficulty in detecting J1909+06 as a periodic source. The inaccuracy of the  $\Delta t_{\text{ISS}}$  estimate stems from the assumed  $V_{\text{ISS}}$  and the fact that NE2001 distance estimates may have errors of up to 20%.

### 7.5. J1919+17

During the 2007 discovery observation of J1919+17, multiple pulses at  $\text{DM} = 148 \text{ pc cm}^{-3}$  were detected in beam 4 of the ALFA receiver, with no corresponding periodic detection. A Fast Folding Analysis (Staelin 1968) was used to narrow down the period to  $P = 2.081$  s, which was confirmed in 2008, when the pulsar was detected as a normal periodic emitter with the more sensitive central ALFA beam. The pulsar has a double-peak profile with the two peaks  $\sim 100$  ms apart, which most likely made it difficult to find its period from pulse arrival times alone.

### 7.6. J1928+15

PSR J1928+15 was discovered in 2005 by detection of what looked like a single bright pulse at  $\text{DM} = 245 \text{ pc cm}^{-3}$  in a 120 s observation (Fig. 3). More detailed analysis revealed that the event was in fact composed of 3 separate pulses occurring at intervals of 0.403 s, with the middle pulse being brighter by an order of magnitude than the other two (Fig. 9). In Fig. 4a the dispersion of the brightest pulse by ionized interstellar gas is shown in the time-frequency plane, evidence of the non-terrestrial origin of the pulses. A fit to the pulse signal in the time-frequency plane resulted in a refined estimate of  $\text{DM} = 242 \text{ pc cm}^{-3}$ . Despite multiple follow-up observations, the source has not been detected again. Its period of 0.403 s is not long enough compared to the discovery observation time for the small- $N_p$  selection effect to be prominent. The higher the pulsar DM ( $\gtrsim 150 \text{ pc cm}^{-3}$ ), the more wavefront modulations due to intervening ionized gas will cancel out statistically, and therefore  $\text{DM} = 242 \text{ pc cm}^{-3}$  rules out scintillation for J1928+15. Since the 3 pulses occurred at successive rotations of the neutron star, they were likely caused by a single magnetospheric event. This is a signature expected from an old pulsar whose emission mechanism is reactivated by sporadic accretion of material from an asteroid belt (Cordes & Shannon 2008). However, old pulsars beyond the death line are expected to have periods on the order of several seconds, which is significantly longer than the period of J1928+15.

### 7.7. J1946+24

PSR J1946+24 has  $DM = 96 \text{ pc cm}^{-3}$  and  $P = 4.729 \text{ s}$  and was discovered by detecting 4 individual pulses. The intervals between detected pulses in this case were all  $> 20 \text{ s}$ , suggesting that they were not emitted on successive rotations of the pulsar. The brightest detected pulse of J1946+24 has  $S/N = 29$  and its dispersion sweep is visible in the time-frequency plane without any stacking (Fig. 4b).

### 7.8. Summary

Single pulse arrival times collected over multiple follow-up observations were used to obtain partial timing solutions for J0628+09, J1909+06, J1919+17, J1854+03 and J1946+24 and verify their estimated periods. The periods of J0627+16 and J1909+06 were verified by manually folding raw data and detecting a periodic signal. Finally, despite the fact that J1928+15 was not detected after the discovery observation, the  $\sim 0.403 \text{ s}$  intervals between the three pulses detected from that source differ by only  $\sim 2 \text{ ms}$ , which is approximately half the FWHM pulse width and therefore provides a period estimate to that precision.

## 8. Constraints on Transient Detections

In addition to making new discoveries and contributing to the overall statistics of known radio pulsars, large surveys like PALFA place constraints on the detectability and rate of Galactic and extragalactic transients which are not necessarily related to rotating neutron stars. In this section we apply constraints derived from the parameters and results of the PALFA survey to isolated and repeating transients and discuss a recent energetic transient detection in the context of these constraints.

If an isolated burst is detected in a single pulse search, the main questions we wish to answer are: how far away is the source, what is the burst luminosity, what are the types of objects that could be its progenitors, and what is the expected rate of similar events over the whole sky.

### 8.1. Repeating Source

If a single event is detected, follow-up observations are necessary in order to reveal whether it is from a repeating source and measure or place limits on the pulse rate. Assuming

a repeating source with a power-law pulse amplitude distribution  $N(S) \propto S^{-\alpha}$  and index  $\alpha > 1$ , the number of detectable events is

$$N(S \geq S_{\min}) = N(S \geq S_{\text{pk}}) \left( \frac{S_{\text{pk}}}{S_{\min}} \right)^{\alpha-1}, \quad (12)$$

where  $S_{\text{pk}}$  is the peak flux density and  $S_{\min}$  is the flux density corresponding to the single pulse detection threshold. In general, the brighter the original event, the more likely it is to detect weaker pulses from the same source if the source repeats. The absence of such detections suggests that the source either repeats on a time scale longer than the follow-up observations or the progenitor was a one-time event.

## 8.2. Isotropic Source Population

Next we consider the possibility that the event progenitor is from an isotropic population of sources. For a survey pointing of solid angle  $\Omega_i = N_{\text{pix}}\Omega_1$  consisting of  $N_{\text{pix}}$  beams covering  $\Omega_1$  of solid angle each, the volume searched per pointing is

$$\Delta V_i = \frac{1}{3}\Omega_i D_{\max}^3, \quad (13)$$

where the maximum detection distance  $D_{\max}$  and actual source distance  $D$  are related through  $D_{\max} = D(S_{\text{pk}}/S_{\min})^{1/2}$ . Let the total survey time  $T_{\text{obs}}$  correspond to the total number of pointings  $N_{\text{pt}}$  with an observation time per pointing of  $T_{\text{obs},i} = T_{\text{obs}}/N_{\text{pt}}$  and bandwidth  $\Delta f$ . For a source number density  $n_s$  and event rate per volume per unit time  $\dot{n}_s$ , the total number of events detected is

$$N = \dot{n}_s T_{\text{obs},i} N_{\text{pt}} \Delta V_i = \frac{1}{3} \dot{n}_s T \Omega_i \left( \frac{L_p}{m S_{\text{sys}}} \right)^{3/2} (N_{\text{pol}} \Delta f W)^{3/4}. \quad (14)$$

To compare surveys, we make use of the fact that  $S_{\text{sys}} = T_{\text{sys}} 2k/A_e$  and  $A_e \Omega_1 = \lambda^2$ , where  $A_e$  is effective telescope area,  $\lambda$  is the observing wavelength and  $k$  is the Boltzmann constant. The ratio of the number of events detected by two surveys is

$$\frac{N_b}{N_a} = \frac{T_{\text{obs},b} N_{\text{pix},b}}{T_{\text{obs},a} N_{\text{pix},a}} \left( \frac{\Omega_{1,a}}{\Omega_{1,b}} \right)^{1/2} \left( \frac{m_a T_{\text{sys},a}}{m_b T_{\text{sys},b}} \right)^{3/2} \left( \frac{\Delta f_b}{\Delta f_a} \right)^{3/4}. \quad (15)$$

Exotic events such as annihilating black holes and coalescing neutron stars are expected to be detectable over extragalactic distances and are of great interest as cosmological probes. If such a transient is detected, comparing expected survey detection rates or limits derived from non-detections can be used to verify its origin.

### 8.3. Far-out Sidelobe Constraints

Celestial and terrestrial radio signals can enter the seven beams of the ALFA receiver indirectly through reflection and scattering off support structures. Very bright signals of both types may be detected after being scattered into one or more beams, and the effective gain would correspond approximately to that of the far-out sidelobes. While in that case it would be difficult to distinguish celestial from terrestrial signals based on whether they are detected in one beam, a subset of beams, or all beams, analysing the time-frequency plane through dedispersion will effectively pick out celestial pulses, which will exhibit a frequency sweep matching the cold-plasma dispersion law.

Antenna power patterns have near-in sidelobes which can be approximated by an Airy function and scale with angle as  $\lambda/D_a$ . Far-out sidelobes are independent of the reflector diameter  $D_a$  and have gains  $G \lesssim 1$ , similar to an isotropic antenna. For the Arecibo telescope, we expect sidelobes to have the same general properties, with the caveat that support structures will introduce further complexity in the far-out sidelobe pattern which varies as the telescope is tracking. In general, peaks in the far-out sidelobe envelope can have gains significantly larger than  $G = 1$ .

The gain can be expanded into main beam and far-out sidelobe terms:

$$G(\theta, \phi) = G_{\max} P_n(\theta, \phi) + (1 - \eta_B), \quad (16)$$

where  $\theta$  and  $\phi$  are elevation and azimuth, respectively,  $P_n(\theta, \phi)$  is the power pattern for the main beam and near-in sidelobes and  $(1 - \eta_B)$  is the average level of the far-out sidelobes. The boresight gain

$$G_{\max} = \frac{4\pi A_e}{\lambda^2} = \frac{4\pi}{\Omega_A} = \frac{4\pi\eta_B}{\Omega_{\text{MB}}}, \quad (17)$$

where  $\Omega_A$  is the antenna power pattern solid angle. Considering one pixel of the ALFA receiver,  $\eta_B$  and  $\Omega_{\text{MB}} = \eta_B\Omega_A$  are the efficiency and solid angle of the main beam plus near-in sidelobes, respectively. In terms of  $G_{\max}$ , the system equivalent flux density is

$$S_{\text{sys}} = \frac{T_{\text{sys}} 2k}{A_e} = \frac{8\pi k T_{\text{sys}}}{\lambda^2 G_{\max}}, \quad (18)$$

and the minimum detectable flux density is given by

$$S_{\min} = \frac{m S_{\text{sys}}}{\sqrt{N_{\text{pol}} \Delta f W}}. \quad (19)$$

For a multibeam receiver, the main lobe and near-in sidelobes of the individual beams cover distinct areas of sky, but the far-out sidelobes essentially overlap and can be approximated by an annulus of solid angle  $\Delta\Omega$  centered on the boresight direction. The number of

events in that solid angle is

$$N = \dot{\zeta}_s T \Delta\Omega, \quad (20)$$

where  $\dot{\zeta}_s$  is the event rate per solid angle. If after a time  $T$  no events are detected, we have  $S \leq S_{\min}$  and we can set a limit  $\dot{\zeta}_s \leq \dot{\zeta}_{s,\max}$ , where  $\dot{\zeta}_{s,\max} = 1/(T\Delta\Omega)$ . For the main beam and near-in sidelobes,  $\Delta\Omega = \pi\theta_{\text{near}}^2$ , where  $\theta_{\text{near}}$  is the angular radius of the near-in sidelobes. For the annulus-like far-out sidelobes,  $\Delta\Omega = 2\pi\theta_{\text{far}}\Delta\theta_{\text{far}}$ , where  $\theta_{\text{far}}$  is the angular distance from boresight to the far-out sidelobes and  $\Delta\theta_{\text{far}}$  is their angular extent. If  $S_{\min,1}$  is the minimum detectable flux density for unit gain, defined as  $S_{\min} \equiv S_{\min,1}/G$ , for the main beam and near-in sidelobes we have

$$S_{\min} = \frac{S_{\min,1}}{G_{\max}} \quad (21)$$

$$\dot{\zeta}_{s,\max} = \frac{1}{\Omega_{\text{MB}}T}, \quad (22)$$

while for large angles  $\theta_{\text{far}}$ , where the far-out sidelobes have an average gain of  $1 - \eta_B$ ,

$$S_{\min} \approx \frac{S_{\min,1}}{1 - \eta_B} \quad (23)$$

$$\dot{\zeta}_{s,\max} = \frac{1}{2\pi\epsilon T}, \quad (24)$$

where  $\epsilon$  is the fraction of the hemisphere actually covered by the far-out sidelobes.

For one beam of the ALFA receiver we have  $\eta_B \approx 0.75$  and  $\Omega_{\text{MB}} = 2.7 \times 10^{-5}$  ster. Fig. 10 shows constraints on event rate and flux density of pulses with  $W = 0.01$  s in a total observation time  $T = 461$  h for the PALFA survey. The assumed antenna power pattern consists of a Gaussian main beam with FWHM of  $3.5'$  approximating the response of one beam of the ALFA receiver, combined with annular far-out sidelobes with an average gain  $1 - \eta_B$ . Within the half-power beam width the constraints are strong on the flux density but weak on the event rate while the opposite is true for the far-out sidelobes, represented by the part of the curve to the left of  $\dot{\zeta} \approx 0.2 \text{ h}^{-1} \text{ deg}^{-2}$ . Because of the dependence of  $S_{\min}$  on the pulse width, for each order of magnitude increase in  $W$  there is half an order of magnitude decrease in the constraint on  $S_{\min}$ .

#### 8.4. An Energetic Transient Detection

Lorimer et al. (2007) report a 30 Jy burst from a direction near the Small Magellanic Cloud detected with the Parkes telescope at 1.4 GHz. Its DM of  $375 \text{ pc cm}^{-3}$  cannot be accounted for by ionized interstellar gas in the Galaxy and the Small Magellanic Cloud.

The finite frequency and time resolution of the filterbank system used in the observation constrain the intrinsic pulse width to  $\lesssim 5$  ms.

The authors argue that the burst originated from a source 500 Mpc away belonging to an isotropically distributed population at cosmological distances, and its high DM is due to a significant contribution from either a host galaxy or intergalactic ionized gas or both. Despite 20 days of total survey time and 90 h of dedicated follow-up observations, no other pulses were detected either from the same direction or anywhere else within the survey area.

Applying Eqn. 12 to this detection and considering that  $S_{\min} \sim 0.3$  Jy for Parkes,  $\sim 10^{2(\alpha-1)}$  events are expected to be above threshold. The absence of weaker pulses suggests that  $\alpha \sim 1$  and/or the source is repeating on a time scale longer than 90 h.

For an isotropic source population, comparing the Parkes Multibeam (PMB) survey of the Galactic plane and the Parkes Magellanic Cloud (MC) survey of Lorimer et al. (2007) using Eqn. 15 yields  $N_{\text{PMB}}/N_{\text{MC}} \sim 4$ . If we make the same comparison between the MC survey and the PALFA survey, the result is of the same order of magnitude,  $N_{\text{PALFA}}/N_{\text{MC}} \sim 2$ . Since the MC survey looked out of the Galactic plane, where the Galactic contribution to dispersion and scattering is small, it is more appropriate to compare it with only the Anticenter portion of PALFA. In that case,  $N_{\text{PALFA}}/N_{\text{MC}} \sim 0.6$ . Overall, the expected PMB and PALFA detection rates for similar events are of order unity for the current survey volume, consistent with the MC survey detecting a single burst in 20 days.

## 8.5. Other Constraints

The 5 ms pulse width of the Lorimer et al. (2007) burst rules out as progenitors phenomena with time scales of minutes to days, such as flares from brown dwarfs or flare stars. Gamma-ray bursts have diverse time scales spanning  $10^{-2} - 10^3$  s and neutron star-neutron star and neutron star-black hole mergers are proposed progenitors of short gamma-ray bursts (Paczynski 1986). However, no gamma-ray burst was detected coincident in time or location with the Lorimer et al. (2007) radio burst. Prokhorov et al. (1997) summarize estimates for the Galactic rate of such mergers from both observational and theoretical constraints and the results span the range  $10^{-6} - 10^{-4}$  yr $^{-1}$  or  $10^{-10} - 10^{-8}$  h $^{-1}$ . Another energetic phenomenon which is expected to produce a single bright pulse is the annihilation of primordial black holes (Rees 1977). O’Sullivan et al. (1978) and Phinney & Taylor (1979) estimate the Galactic rate for such events to be  $2 \times 10^{-9} - 9 \times 10^{-9}$  pc $^{-3}$  yr $^{-1}$ . Taking into account the PALFA survey coverage from Table 1, the numbers for both compact object mergers and primordial black hole annihilation are well within the allowed region from Fig. 10.



Katz et al. (1998) and Balsano (1999) performed a targeted search for prompt radio emission from gamma-ray bursts at 611 MHz and 76 MHz respectively, and based on the absence of any definitive detections estimate  $S < 10^4 - 10^5$  Jy. Hansen & Lyutikov (2000) derive properties of radio counterparts of neutron star-neutron star mergers and suggest an expected flux density of  $\sim 5$  Jy at 400 MHz for  $D \sim 100$  Mpc. Even assuming a flat spectrum, the former is very close to our far-out sidelobe limit for  $S_{\min}$ , and the latter could only be detected by the main beam.

In conclusion, the rarity of compact object mergers and black hole annihilations per galaxy make it unlikely that the Lorimer et al. (2007) burst was generated by such an exotic event within or near the Milky Way. Considering the low number of main beam detections similar to the burst expected from either the PALFA or Parkes Multibeam surveys, the absence of such detections so far does not constrain the burst origin.

## 9. Conclusions

We have examined the current state of knowledge about various classes of intermittent radio-loud neutron stars, summarized selection effects which may affect the classification of intermittent sources, and presented our data processing methods and results from single pulse searches performed on PALFA survey data. One of our single pulse discoveries was found to be a steady emitter likely affected by scintillation (J1909+06), and two sources were detected as normal periodic emitters when observed at a lower frequency (J0627+16) and with the more sensitive central beam of the ALFA receiver (J1919+17). Four objects were most likely not detected via periodicity search because of their long periods ( $P > 2$  s) compared to the PALFA observation time of 134 – 268 s, and one intermittent object (J1928+15) was discovered by detecting three pulses emitted on successive rotations but it was not detected again despite multiple reobservations. The wide variety of observational properties exhibited by these single pulse sources and the influence of selection effects on their detectability indicate that some intermittent emission signatures can be explained as due to observational biases. Detailed follow-up analysis is necessary to separate them from the objects whose intermittency may be due to intrinsic physical differences from the normal pulsar population.

Some sources appear to correspond to one-time physical events or to be intermittent on a much longer time scale than others. Two series of bursts were detected in the J1839–01 discovery observation, and none in multiple follow-up observations. For all Parkes intermittent sources except J1839–01 an average burst rate has been measured and verified through follow-up observations. All PALFA single pulse sources except J1928+15 also exhibit a spread of pulses over observation time and reobservations confirmed their burst rates and

rotation periods.

Based on these properties, most of the combined Parkes and PALFA sample of single pulse sources are *sporadic* but have measurable and consistent pulse rates. J1928+15 may belong to an observational (and possibly also physical) class of *serendipitous* intermittent objects, and J1839–01 seems to stand on its own between these two observational classes of transients. Serendipitous radio transients may have a signature which consists of only one burst or a single sequence of pulses. If several pulses arrive in succession, a rotation period can be determined and the emitting object identified as a rotating neutron star which may be undergoing a magnetospheric event that activates a dormant or intensifies an existing emission mechanism. Various energetic physical events such as supernova explosions and coalescing black holes or neutron stars may be detectable as serendipitous, isolated radio bursts at galactic and extragalactic distances.

If we only see transients once, how can we figure out what phenomena produce them? We must archive radio survey data and characterize the wide variety of detected radio transients outside the framework of rotating neutron stars if necessary. Archived data may yield new discoveries if reprocessed with improved search algorithms and a database of transient signals would be an invaluable reference as theoretical understanding of energetic radio events and prediction of their signatures improves. The PALFA survey is taking steps in both directions: raw data are stored in a tape archive and data processing products are indexed in a database at the Cornell Center for Advanced Computing and currently work is under way to make them publicly available via a web portal.<sup>3</sup>

We thank the staff at NAIC and ATNF for developing the ALFA receiver and the associated backend systems. In particular, we thank Jeff Hagen, Bill Sisk and Steve Torchinsky at NAIC and Graham Carrad at the ATNF. We are also grateful to the Parkes Multibeam survey team for providing the results incorporated in Fig. 8. This work was supported by the NSF through a cooperative agreement with Cornell University to operate the Arecibo Observatory. NSF also supported this research through grants AST-02-05853 and AST-05-07376 (Columbia University), AST-02-06035 and AST-05-07747 (Cornell University) and AST-06-47820 (Bryn Mawr College). M.A.M., D.R.L. and P.C.C.F. are supported by a WVEPSCoR Research Challenge Grant. M.A.M. is an Alfred P. Sloan Research Fellow. F. Crawford is supported by grants from Research Corporation and the Mount Cuba Astronomical Foundation. Pulsar research at UBC is supported by NSERC and the Canada Foundation for Innovation. L.E.K. held an NSERC Canada Graduate Scholarship while most of this work

---

<sup>3</sup><http://arecibo.tc.cornell.edu>

was performed. V.M.K. holds a Canada Research Chair and the Lorne Trottier Chair, and is supported by NSERC, FQRNT, CIFAR, and by the Canada Foundation for Innovation. The Parkes telescope is part of the Australia Telescope, which is funded by the Commonwealth Government for operation as a National Facility managed by CSIRO. NRAO is a facility of the NSF operated under cooperative agreement by Associated Universities, Inc. Research in radio astronomy at the NRL is supported by the Office of Naval Research.

## REFERENCES

- Backer D.C. 1970, *Nature*, 228, 42
- Balsano R.J. 1999, PhD Thesis, Princeton University
- Berger, E. 2002, *ApJ*, 572, 503
- Berger, E. et al. 2001, *Nature*, 410, 338
- Bhat N.D.R., Cordes J.M., Camilo F., Nice D.J. & Lorimer D.R. 2004, *ApJ*, 605, 759
- Champion, D. J. et al. 2008, *Science*, 320, 1309
- Cordes J.M. & Lazio T.J.W. 2002, astro-ph/0207156
- Cordes J.M. et al. 2006, *ApJ*, 637, 446
- Cordes J.M. & McLaughlin, M.A. 2003, *ApJ*, 596, 1142
- Cordes J.M. & Rickett B.J. 1998, *ApJ*, 507, 846
- Cordes J.M. & Shannon R.M. 2008, *ApJ*, 682, 1152
- D’Amico, N., Possenti, A., Manchester, R. N., Sarkissian, J., Lyne, A. G. & Camilo, F. 2001, *ApJ*, 561, L89
- Deich, W. T. S., Cordes, J. M., Hankins, T. H. & Rankin, J. M. 1986, *ApJ*, 300, 540
- Dowd, A., Sisk, W., Hagen, J. 2000, *ASPC*, 202, 275
- Farrell, W. M., Desch, M. D., & Zarka, P. 1999, *JGR*, 104, 14025
- Fender, R. P., Bell Burnell, S. J., Waltman, E. B., Pooley, G. G., Ghigo, F. D., & Foster, R. S. 1997, *MNRAS*, 288, 849
- Fruchter, A. S., Stinebring, D. R. & Taylor, J. H. 1988, *Nature*, 333, 237

- Garcia-Sanchez, J., Paredes, J. M., & Ribó, M. 2003, *A&A*, 403, 613
- Gupta Y. 1995, *ApJ*, 451, 717
- Hankins T. H., Kern J. S., Weatherall J. C., Eilek J. A., 2003, *Nature*, 422, 141
- Hansen M.S. & Lyutikov, M. 2000, *MNRAS*, 322, 695
- Hessels, J. W. T. et al. 2008, *ApJ*, 682, L41
- Huchra, J. P. & Geller, M. J. 1982, *ApJ*, 257, 423
- Jackson, P. D., Kundu, M. R., & White, S. M. 1989, *A&A*, 210, 284
- Johnston, S., van Straten, W., Kramer, M., & Bailes, M. 2001, *ApJ*, 549, L101
- Kaspi, V. M., Ransom, S. M., Backer, D. C., Ramachandran, R., Demorest, P., Arons, J. & Spitkovsky, A. 2004, *ApJ*, 613, L137
- Katz C.A., Hewitt J.N., Moore C.B. & Corey B.E. 1998, *AIP Conf. Proc.*, 428, 581
- Lazio, T. J. W., Farrell, W. M., Dietrick, J., Greenlees, E., Hogan, E., Jones, C., Hennig, L. A. 2004, *ApJ*, 612, 511
- Lewandowski W., Wolszczan A., Feiler G., Konacki M. & Soltysinski T. 2004, *ApJ*, 600, 905
- Lorimer, D. R. et al. 2006, *ApJ*, 640, 428
- Lorimer D.R., Bailes M., McLaughlin M.A., Narkevic D.J. & Crawford F. 2007, *Science*, 318, 777
- Lyne, A. G., Johnston, S., Manchester, R. N., Staveley-Smith, L. & D’Amico, N. 1990, *Nature*, 347, 650
- Lyne, A. G., Biggs, J. D., Harrison, P. A. & Bailes, M. 1993, *Nature*, 361, 47
- Knight, H. S. 2006, *ChJAA*, 6, 41
- Kramer M., Lyne A.G., O’Brien J.T., Jordan C.A. & Lorimer D.R. 2006, *Science*, 312, 549
- Manchester, R. N., Lyne, A. G., Camilo, F., Bell, J. F., Kaspi, V. M., D’Amico, N., McKay, N. P. F., Crawford, F., Stairs, I. H., Possenti, A., Kramer, M., Sheppard, D. C. 2001, *MNRAS*, 328, 17
- Manchester, R. N., Hobbs, G. B., Teoh, A. & Hobbs, M. 1993-2006 (2005) *AJ*, 129

- McLaughlin M.A. & Cordes J.M. 2003, ApJ, 596, 982
- McLaughlin, M. A. et al. Nature, 439, 817
- McLaughlin, M. A., Rea, N., Gaensler, B. M., Chatterjee, S., Camilo, F., Kramer, M., Lorimer, D. R., Lyne, A. G., Israel, G. L., Possenti, A. 2007, ApJ, 670, 1307
- Nice, D. J. 1999, ApJ, 513, 927
- O’Sullivan J.D., Ekers R.D. & Shaver P.A. 1978, Nature, 176, 590
- Paczynski B. 1986, ApJ, 308, L43
- Phinney S. & Taylor J.H. 1979, Nature, 277, 117
- Popov M. V., Soglasnov V. A., Kondratiev V. I., Kostyuk S. V., 2004, Astronomy Letters, 30, 95
- Prokhorov M.E., Lipunov V.M. & Postnov K.A. 1997, VHEP Conf. Proc., ISBN: 2-86332-217-6
- Rees, M. J. 1977, Nature, 266, 333
- Reynolds, S.P. et al. 2006, ApJ, 639L, 71
- Sagiv, A. & Waxman, E. 2002, ApJ, 574, 861
- Soglasnov, V. A., Popov, M. V., Bartel, N., Cannon, W., Novikov, A. Yu., Kondratiev, V. I. & Altunin, V. I. 2004, ApJ, 616, 439
- Staelin, D. H. 1968, Proc. IEEE, 57, 724
- Stappers, B. W., Bailes, M., Lyne, A. G., Manchester, R. N., D’Amico, N., Tauris, T. M., Lorimer, D. R., Johnston, S. & Sandhu, J. S. 1996, ApJ, 465, L119
- Usov, V. V. & Katz, J. I. 2000, A&A, 364, 655
- Waltman, E. B., Ghigo, F. D., Johnston, K. J., Foster, R. S., Fiedler, R. L., & Spencer, J. H. 1995, AJ, 110, 290
- Wang, N., Manchester, R. N., Johnston, S. 2006, MNRAS, 377, 1383
- Weltevrede P., Stappers B.W., Rankin J.M. & Wright G.A.E. 2006, ApJ, 645L, 149
- Zarka, P., Farrell, W. M., Kaiser, M. L., Blanc, E., Kurth, W. S. 2004, P&SS, 15, 1435



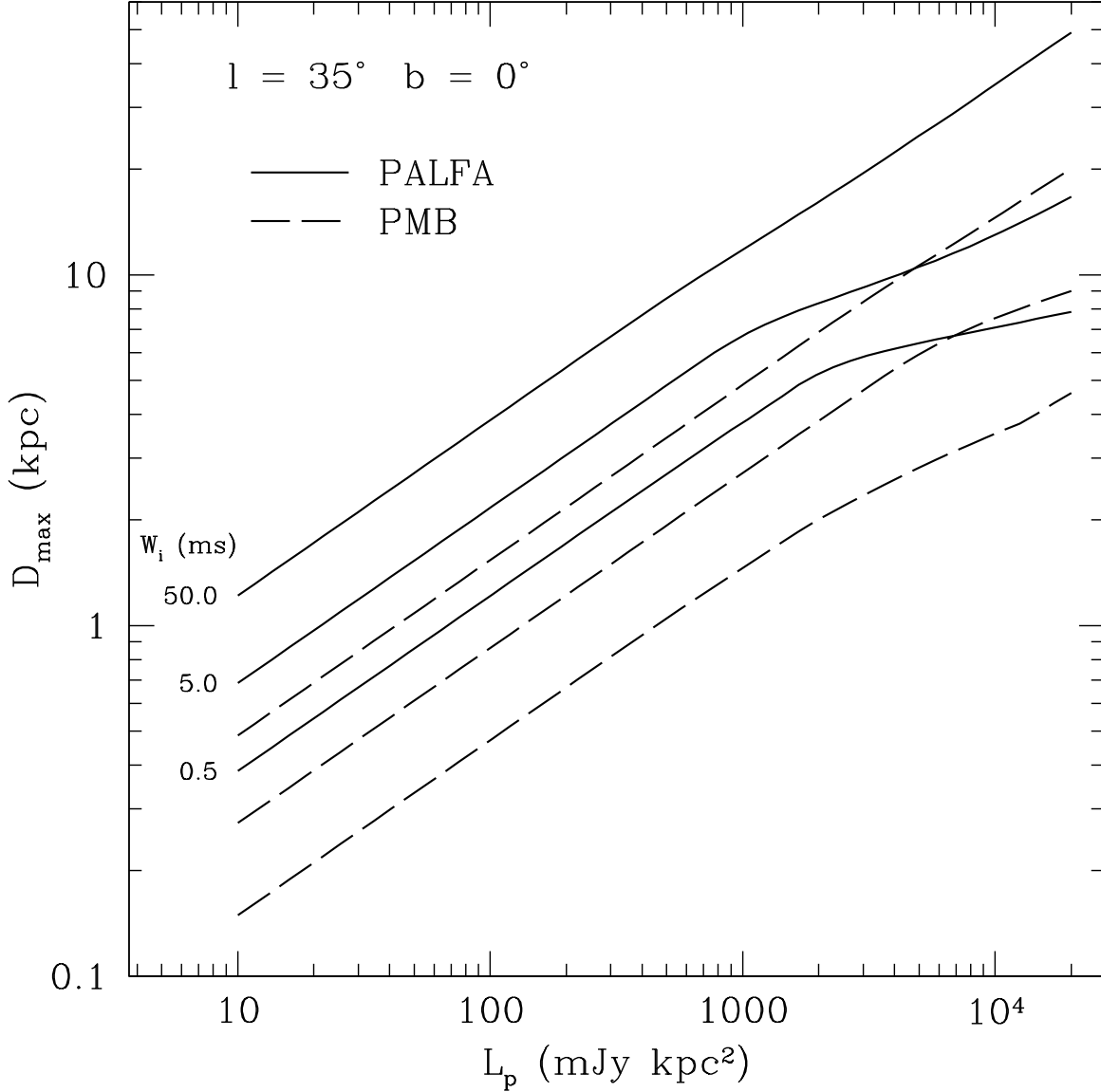


Fig. 1.— Maximum distance at which transients with various peak luminosities and pulse widths of (top to bottom) 50, 5, and 0.5 ms can be detected by the PALFA and Parkes Multibeam surveys. Breaks in the curves correspond to a transition from a luminosity-limited to a scattering-limited detection regime. In the luminosity-limited regime,  $D_{\max}$  is about twice larger for PALFA than for the Parkes Multibeam survey because of the larger sensitivity of the Arecibo telescope. The transition to a scattering-limited regime occurs at lower luminosities for PALFA because of the smaller channel width (0.4 MHz) compared to Parkes (3 MHz).

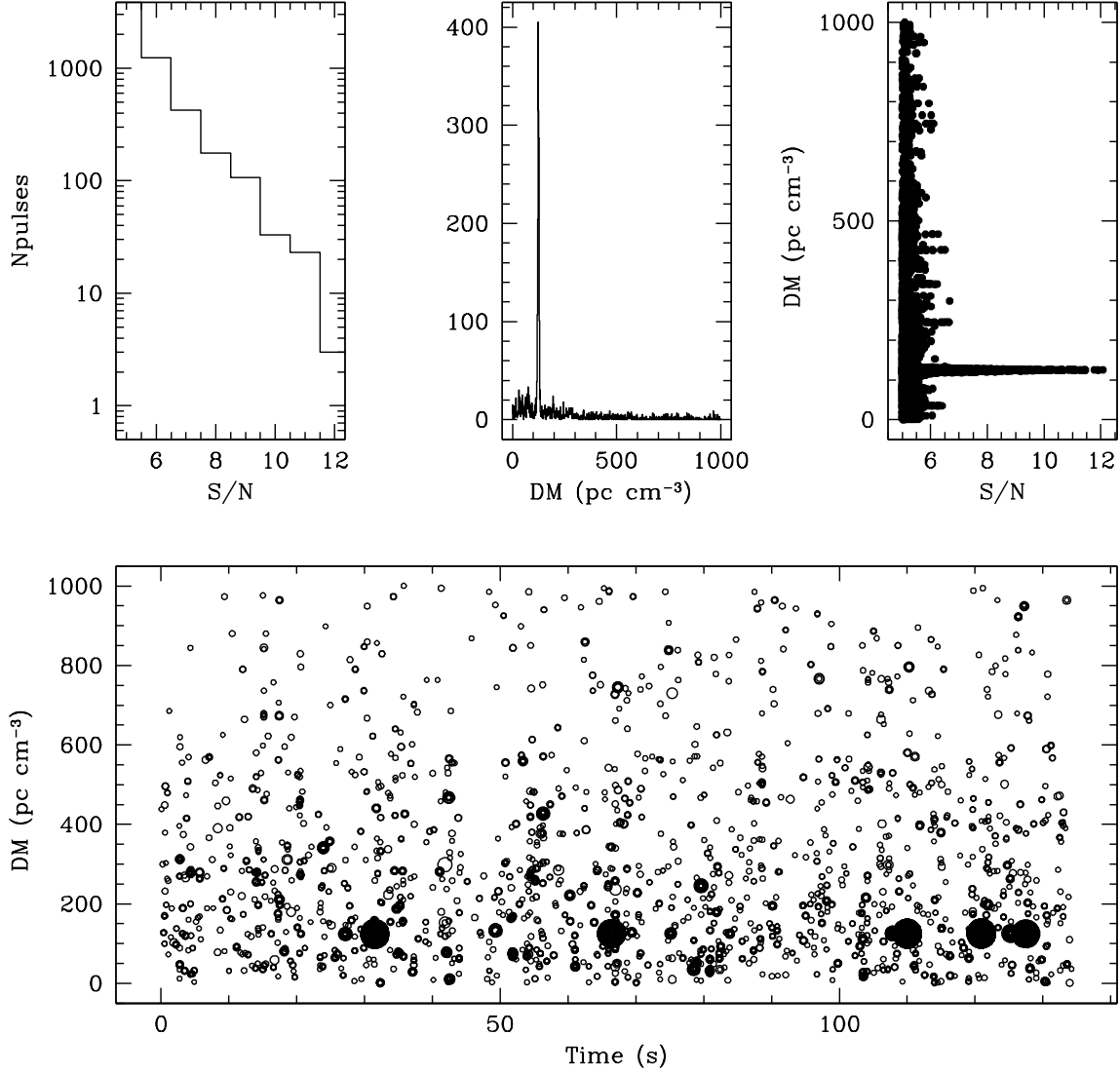


Fig. 2.— Single pulse search output for J0627+16. The bottom panel shows events with  $S/N > 5$  vs. time and DM with larger circles denoting brighter bursts. Panels on top from left to right show histograms of the number of events vs.  $S/N$  and DM, and a scatter plot of event DM vs.  $S/N$ . A fit to the narrow peak of event DM vs.  $S/N$  indicates a pulse width  $\sim 2$  ms (Cordes & McLaughlin 2003).



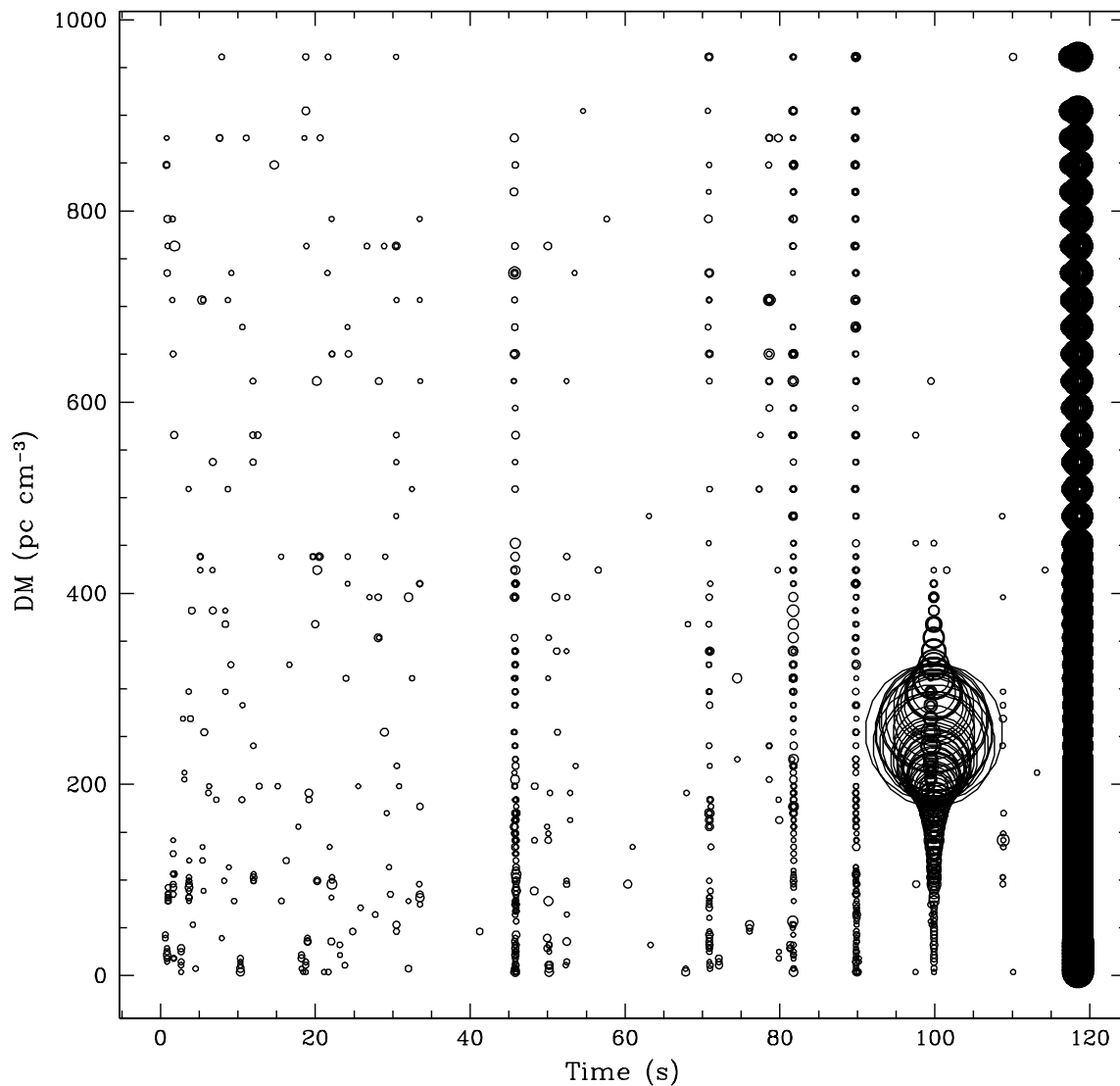


Fig. 3.— Events with  $S/N > 4$  from the discovery PALFA observation of J1928+15 displayed in the DM-time plane. Three closely spaced bursts were found at  $t \sim 100$  s,  $DM \sim 250$  pc  $cm^{-3}$ . Larger circles denote brighter bursts, and the brightest burst has  $S/N \sim 60$ . Events aligned vertically and spanning all trial DM values at  $t \sim 46, 82, 90, 118$  s are due to radar interference.

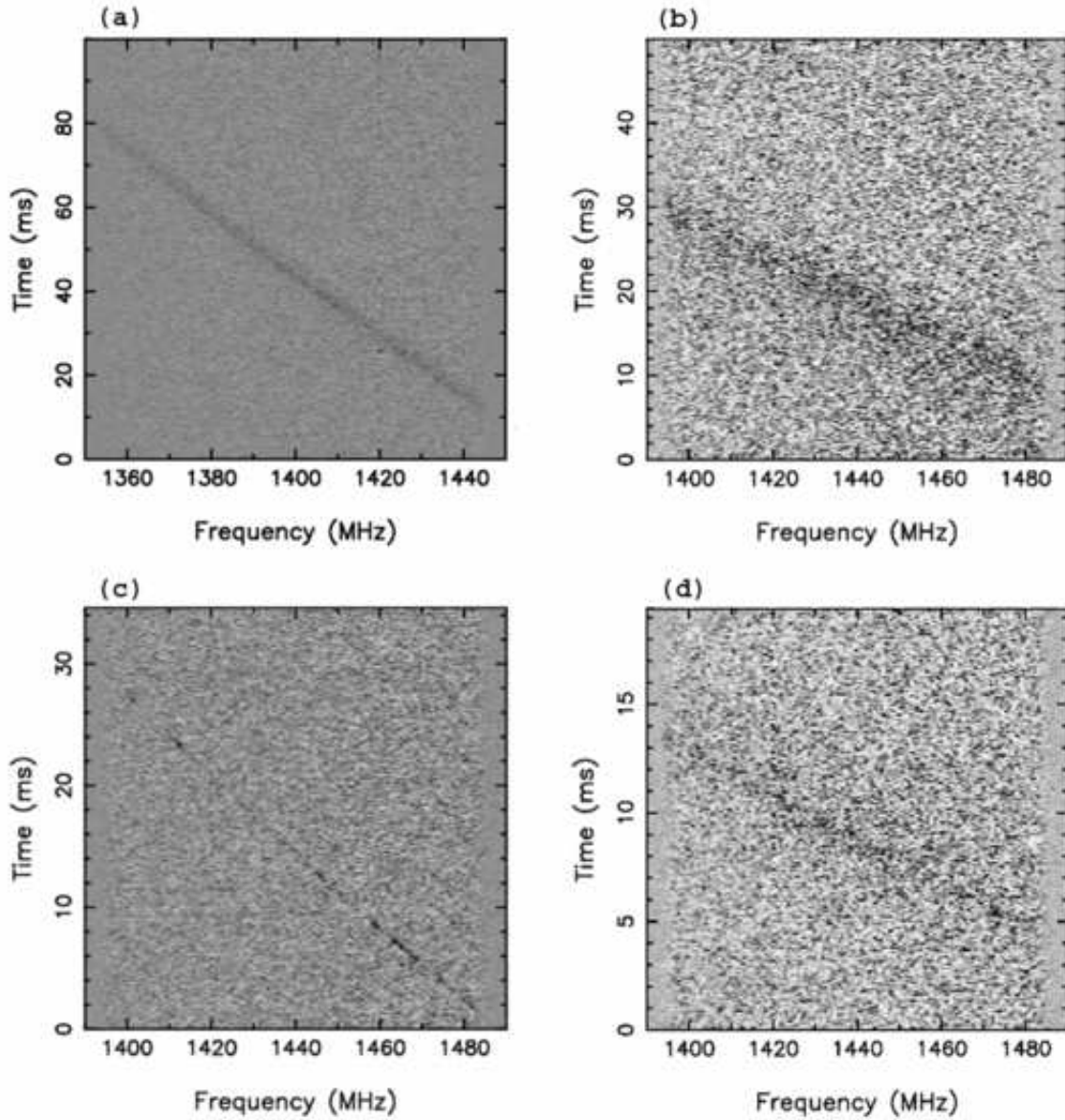


Fig. 4.— Dispersion sweep in the time-frequency plane of the brightest single pulse detected from (a) J1928+15 and (b) J1946+24. (c) Cumulative dynamic spectrum of the five brightest pulses detected from J0627+16. (d) Cumulative dynamic spectrum of the two brightest pulses detected from J1909+06. The pulses are dispersed, such that the higher frequencies arrive earlier.

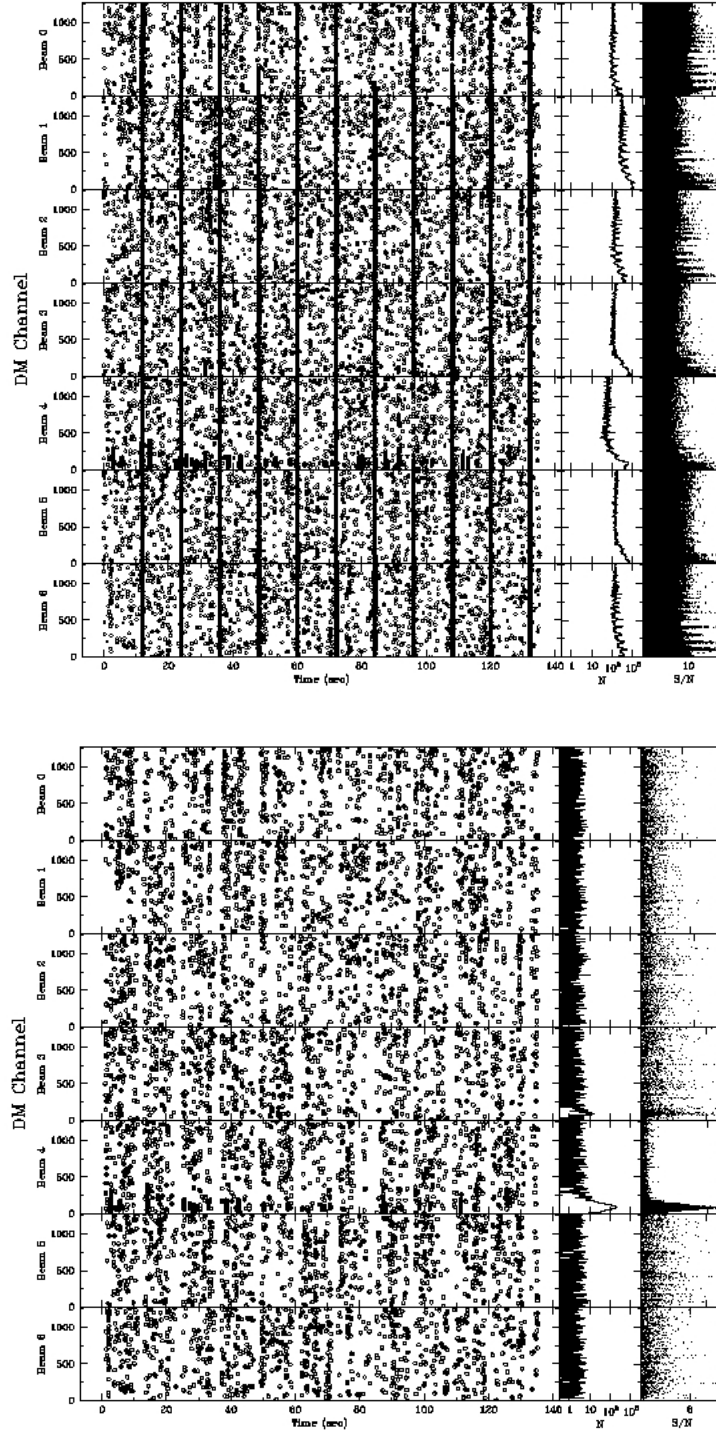


Fig. 5.— Single pulse search output for a blind detection of pulsar B2020+28 before (top) and after (bottom) excising radar and incidental RFI. Each row shows results from one ALFA beam. From left to right, panels show: events with  $S/N > 5$  vs. DM channel and time, number of events vs. DM channel, and event  $S/N$  vs. DM channel. The pulsar detection in beams 3 and 4 is evident after RFI events are excised.

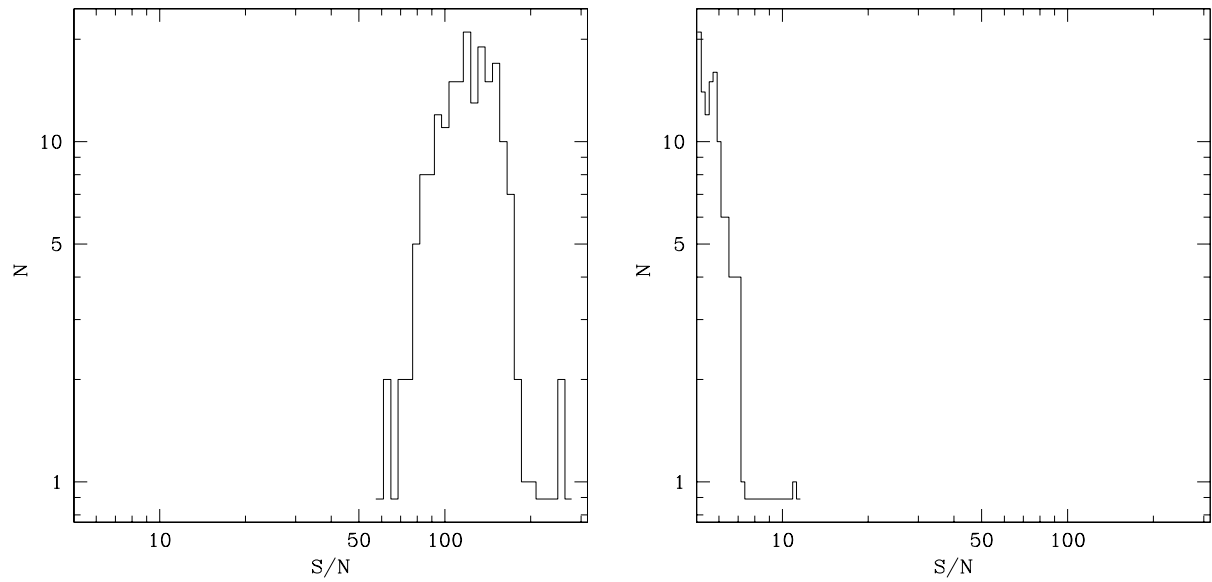


Fig. 6.— Observed single pulse intensity distributions for B1933+16 in two beams of a PALFA pointing: on source (left) and 6 arc minutes away (right). All pulses are detected individually in the on-source beam, while only the high intensity tail of the distribution is detected via a single pulse search in the off-source beam. A sidelobe detection of a normal pulsar will pick out the brightest pulses and may misrepresent the pulsar as an intermittent source.

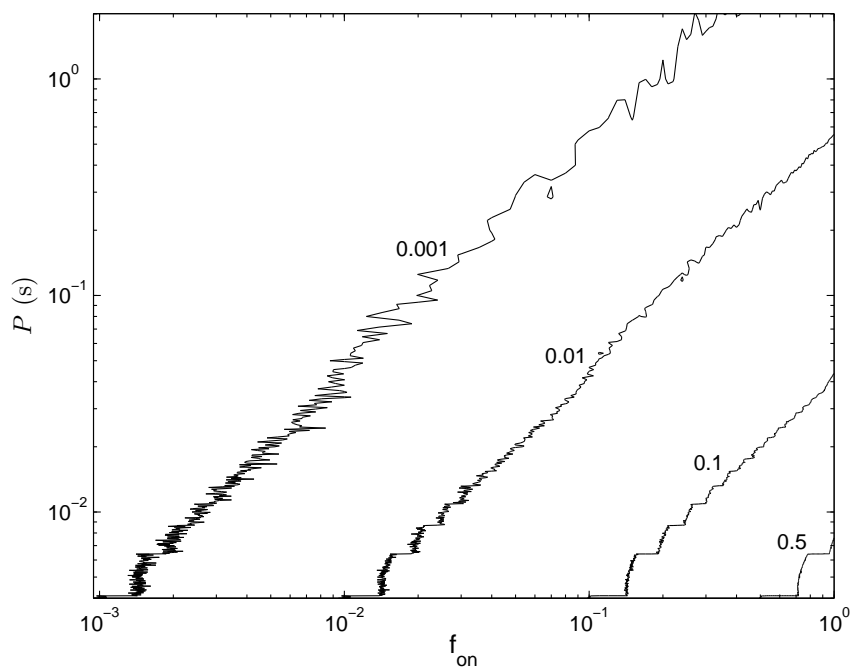


Fig. 7.— Contours of harmonic sum  $H(N_h)$  vs. period and fraction of “on” pulses for  $T_{obs} = 268$  s,  $W = 1$  ms and  $N_h = 1 - 16$  (the value giving the highest  $H(N_h)$  is chosen). A constant unity amplitude was assumed for all “on” pulses. The lines denote regions at 0.1%, 1%, 10% and 50% of the maximum. The precipitous decline in harmonic sum magnitude as  $P$  increases and  $f_{on}$  decreases highlights the difficulty in detecting long-period pulsars as periodic emitters even when pulses are mostly on.

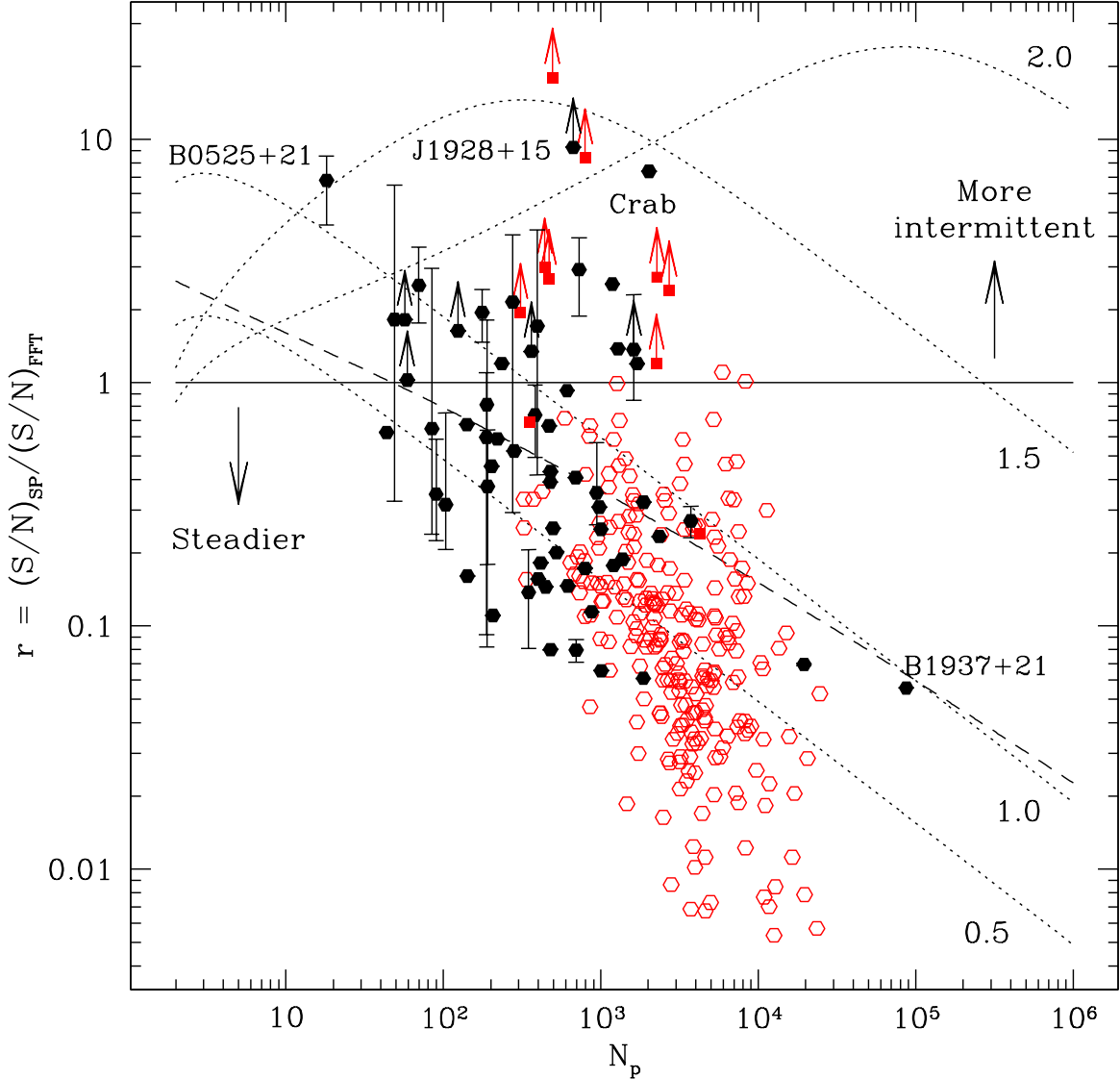


Fig. 8.— The intermittency ratio  $r$  vs  $N_p = T_{r\text{obs}}/P$  for 283 PALFA (filled hexagons) and 255 Parkes Multibeam (squares, open hexagons) pulsar detections. The criterion for inclusion was a simultaneous periodic and single pulse detection. PALFA points include both blind survey detections and targeted test observations of known pulsars. Arrows denote lower limits for PALFA and Parkes intermittent sources for which the period has been determined. Points with bars show the average  $r$  for a set of observations of the same object, with the bars denoting the maximum and minimum  $r$  values. Millisecond pulsar detections appear at lower right. Dotted lines show  $r$  for power-law pulse intensity distributions with indices from 0.5 to 2.0. A ratio of  $10^5$  was assumed for the cutoff intensities  $S_1$  and  $S_2$  (McLaughlin & Cordes 2003). The dashed line shows  $r$  for an exponential pulse intensity distribution. Single pulse search performs better than an FFT periodicity search for  $r > 1$ .

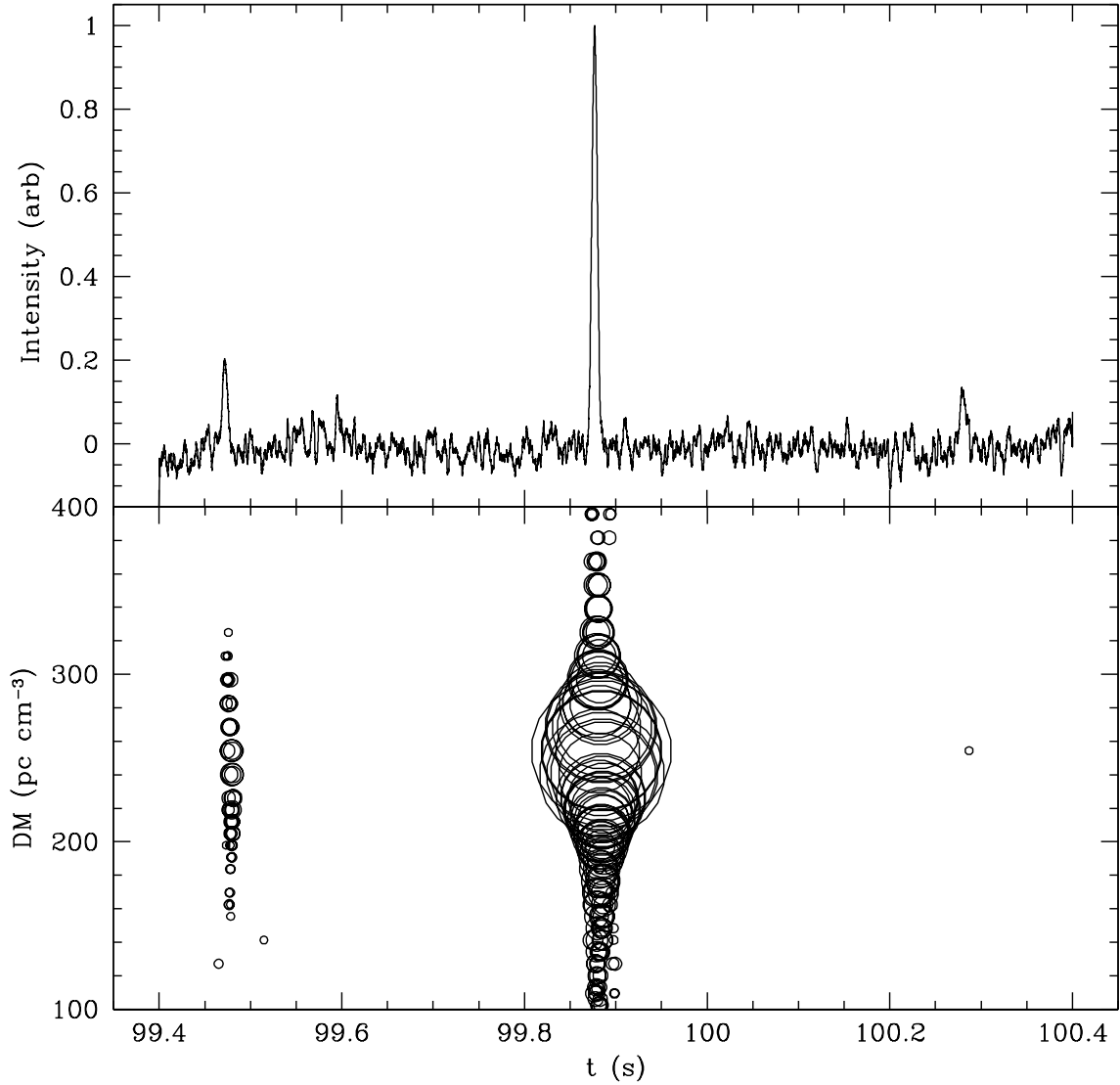


Fig. 9.— The region around  $t \sim 100$  s containing the three bursts from J1928+15 in Fig. 3 is shown magnified here. The intervals between successive bursts are 0.403 s, establishing the pulsar period. The upper panel shows the dedispersed time series, and the lower panel shows the pulses in the DM-time plane. The brightest pulse has  $S/N = 60$  in the dedispersed time series.

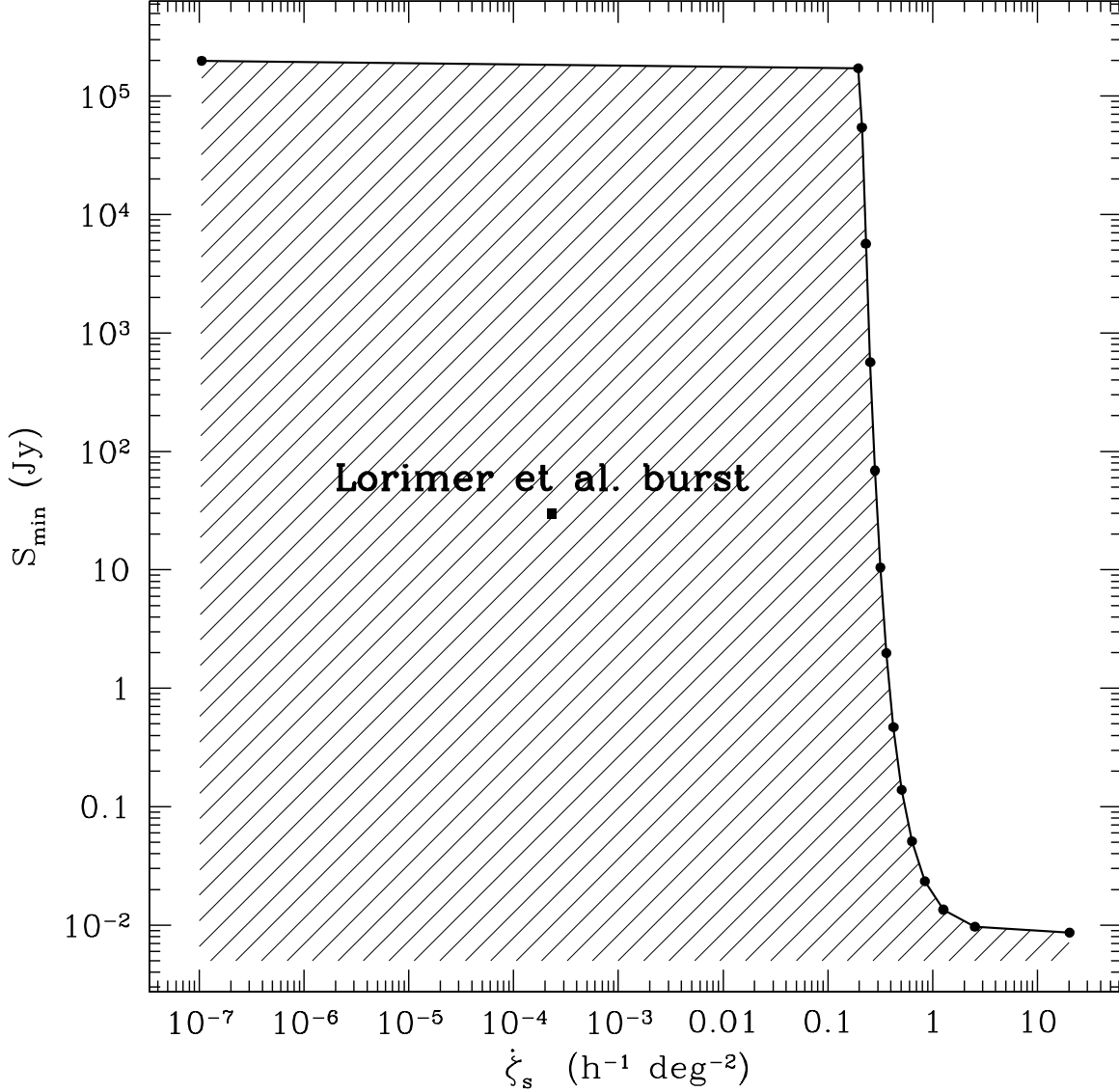


Fig. 10.— Plot of constraints on the single pulse event rate per hour per solid angle  $\dot{\zeta}_s$  for a total observation time  $T = 461$  h and on the minimum detectable flux density  $S_{min}$  for the PALFA survey. The assumed pulse width is  $W = 10$  ms, and the break in the curve at  $\dot{\zeta}_s \approx 0.2 \text{ h}^{-1} \text{ deg}^{-2}$  corresponds to the transition between the main beam and far-out sidelobes. The event rate and flux density are constrained to the shaded region. The event rate inferred by Lorimer et al. (2007) for a cosmological population of 30 Jy bursts is shown within the shaded region.